JCI The Journal of Clinical Investigation

C16ORF70/Mytho promotes healthy ageing in *C. elegans* and prevents cellular senescence in mammals

Anais Franco-Romero, … , Eva Trevisson, Marco Sandri

J Clin Invest. 2024. https://doi.org/10.1172/JCI165814.

Research In-Press Preview Aging Cell biology

Graphical abstract

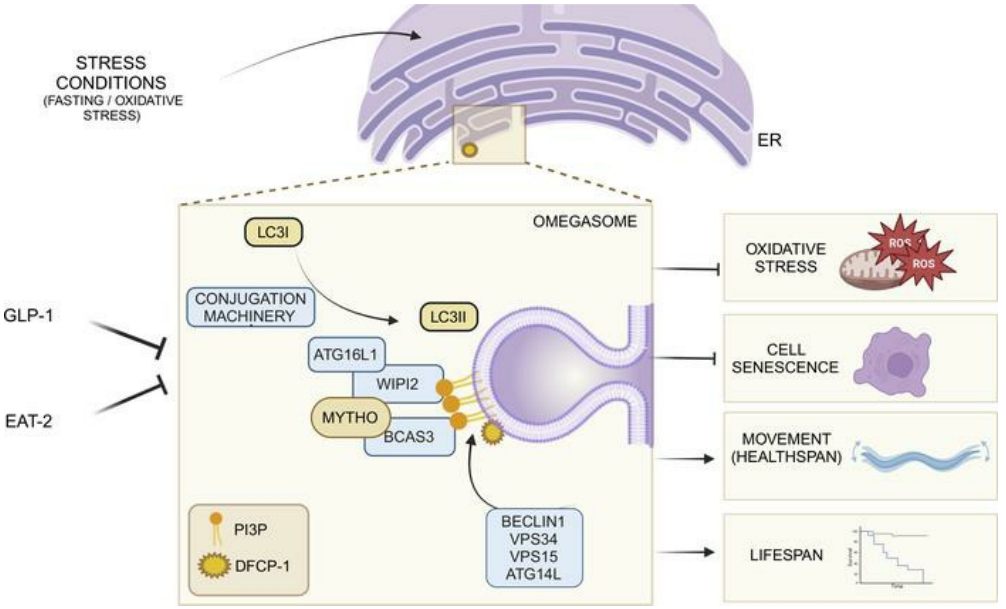

C16ORF70/Mytho promotes healthy ageing in *C. elegans* and prevents cellular senescence in mammals.

Anais Franco-Romero[1,2#], Valeria Morbidoni[3,4#], Giulia Milan[5], Roberta Sartori[1,2], Jesper Wulff[6], Vanina Romanello[1,2], Andrea Armani[1,2], Leonardo Salviati[3,4], Maria Conte[7], Stefano Salvioli[7,8], Claudio Franceschi[9], Viviana Buonomo[10], Casey O. Swoboda[11, 12],-Paolo Grumati [10,13], Luca Pannone[14], Simone Martinelli[14], Harold B.J. Jefferies[15], Ivan Dikic[6,16], Jennifer Van der Laan[17,18] , Filipe Cabreiro[17, 18], Douglas P. Millay[11, 19], Sharon A. Tooze[15], Eva Trevisson[3,4*], Marco Sandri[1,2,20,21,22*]

[1] Department of Biomedical Sciences, University of Padova, via U. Bassi 58b, 35121 Padova, Italy.[2] Veneto Institute of Molecular Medicine, via Orus 2, 35129 Padova, Italy. [3]Clinical Genetics Unit, Department of Women's and Children's Health, University of Padova, via Giustiniani 3, 35128 Padova, Italy. [4] IRP Città della Speranza Corso Stati Uniti 4 35127 Padova, Italy. [5] Department of Cardiac Surgery, University Hospital Basel, Basel, Switzerland; Department of Biomedicine, University of Basel, Basel, Switzerland [6] Institute of Biochemistry II, Goethe University Frankfurt - Medical Faculty, University Hospital, Theodor Stern Kai 7, 60590 Frankfurt am Main, Germany. [7] Department of Medical and Surgical Science (DIMEC), University of Bologna, via San Giacomo 12, 40126 Bologna, Italy. [8] IRCCS Azienda Ospedaliero-Universitaria di Bologna, via San Giacomo 12, 40126, Bologna, Italy [9]Institute of Information Technologies, Mathematics and Mechanics, Lobachevsky State University, Nizhny Novgorod, Russia [10] Telethon Institute of Genetics and Medicine (TIGEM), via Campi Flegrei 34, 80078 Pozzuoli, Italy. [11] Division of Molecular Cardiovascular Biology, Cincinnati Children's Hospital Medical Center, Cincinnati, OH, USA.[12] Division of Biomedical Informatics, Cincinnati Children's Hospital Medical Center, Cincinnati, OH, 10 USA. [13] Department of Clinical Medicine and Surgery, University of Naples Federico II, via Pansini 5, 80131 Naples, Italy. [14] Department of Oncology and Molecular Medicine, Istituto Superiore di Sanità, Rome, Italy. [15] The Francis Crick Institute, Molecular Cell Biology of Autophagy, 1 Midland Road, London, NW1 1AT, UK nb vu8. [16] Buchmann Institute for Molecular Life Sciences, Goethe University Frankfurt - Riedberg Campus, 60438 Frankfurt am Main, Germany. [17] CECAD Research Cluster, University of Cologne, Joseph-Stelzmann-Straße 26, 50931 Cologne, Germany. [18]Institute of Clinical Sciences, Imperial College London, Hammersmith Hospital Campus, Du Cane Road, London W12 0NN, UK. [19] Department of Pediatrics, University of Cincinnati College of Medicine, Cincinnati, OH, USA. [20] Myology Center, University of Padova, via G. Colombo 3, 35100 Padova, Italy. [21] Department of Medicine, McGill University, Montreal, Canada. [22] Department of Pharmacology & Therapeutics, College of Medicine, University of Florida, USA.

Co-first authors

*Address correspondence to: Marco Sandri. Department of Biomedical Sciences, University of Padova, via Ugo Bassi 58/B, 35121 Padova, Italy. Phone: +390498716363, Fax: +39 049 7923250; e-mail: marco.sandri@unipd.it , Eva Trevisson: e-mail: eva.trevisson@unipd.it

Declaration of interests: The authors have declared that no conflict of interest exists.

The identification of genes that confer either extension of lifespan or accelerate age-related decline was a step forward in understanding the mechanisms of ageing and revealed that it is partially controlled by genetics and transcriptional programs. Here we discovered that the human DNA sequence *C16ORF70* encoded for a protein, named MYTHO (Macroautophagy and YouTH Optimizer), which controls life- and health-span. *MYTHO* protein is conserved from *C.elegans* to humans and its mRNA was upregulated in aged mice and elderly people. Deletion of the ortholog *myt-1* gene in *C. elegans* dramatically shortened lifespan and decreased animal survival upon exposure to oxidative stress. Mechanistically, MYTHO is required for autophagy likely because it acts as a scaffold that binds WIPI2 and BCAS3 to recruit and assemble the conjugation system at the phagophore, the nascent autophagosome. We conclude that *MYTHO* is a transcriptionally regulated initiator of autophagy that is central in promoting stress resistance and healthy ageing.

Key words: Ageing, senescence, proteostasis, autophagy, protein breakdown, ATG7, WIPI2, oxidative stress, skeletal muscle, sarcopenia, muscle wasting, lifespan, health span.

INTRODUCTION

In nature, organisms are continuously exposed to environmental stresses that challenge their survival. The species that quickly and efficiently adapt to hostile conditions are positively selected. This response is regulated by evolutionary conserved signalling pathways that promote transcriptional changes, which in turn limit tissue damage and foster repair and stress resistance (1). *C. elegans* is an invaluable animal model commonly employed to decipher the molecular and genetic basis for longevity and ageing. Two of the first identified long-lived *C. elegans* mutants carried mutations in genes involved in the insulin/IGF-1 signaling pathway: *daf-2* and *age-1* (2, 3). Mutation in *daf-2*, which is the *C. elegans* homologue of the mammalian insulin/IGF-1 receptor (IGFR), was demonstrated to more than double lifespan. This expanded longevity requires the activity of the FoxO transcription factor *daf-16* (4, 5). In this scenario, FoxOs regulate several stress response pathways and consequently are critical to restrain ageing and promote longevity (6, 7). Another longevity player of the insulin/IGF-1 signaling pathway is *age-1*. It encodes the catalytic subunit of class-I phosphatidylinositol 3-kinase which catalyzes conversion of phosphatidylinositol 4,5-bisphosphate (PIP2) into phosphatidylinositol 3,4,5-trisphosphate (PIP3) (8).

A general cause of cellular senescence and organism ageing is the progressive accumulation of dysfunctional organelles and cellular damages. Impairment of proteostasis alters the protein quality control systems leading to the accumulation of aberrant and dysfunctional macromolecules and is considered among the primary hallmarks of ageing (9). All cells take advantage of an array of mechanisms to preserve the stability and functionality of their proteins or to remove them when they are irreversibly damaged. One of the most important cellular housekeeping and pro-survival pathway is macroautophagy, hereafter named autophagy, whose main action is to remove damaged proteins/organelles and generate molecules that sustain cellular core metabolism. Autophagy contributes to prolong lifespan and health span in mammals (10-13) by removing damaged organelles allowing for the rejuvenation of cellular components. Consistently, inhibition of autophagy results in disease onset and premature senescence in mammals (12). The process of autophagosome formation is catalysed by a complex machinery that contains protein and lipid kinases, membrane binding and lipid transfer proteins, and ubiquitin-like conjugation systems (14). How these components are assembled and act in an ordered manner to generate autophagosomes is still unclear (15, 16). Interestingly, the

environmental clues that promote autophagy activation are also potent stimulators of FoxO in yeast and mammalian cells (17).

However, how context-dependent molecular networks contribute to limit tissue damage, promote repair and, ultimately, longevity remains unclear. This is partially a consequence of the fact that many potential protein-encoding genes in the human genome are still uncharacterised. Indeed, recent metanalysis studies show that of our 20,000 protein-encoding genes, more than 5,000 are still uncharacterised (18). Here we report on the identification of a gene that is conserved from *C. elegans* to humans and plays a critical role in promoting autophagy, stress resistance and healthy ageing.

RESULTS

MYTHO is a highly conserved gene that is induced in ageing.

To identify uncharacterized factors that control ageing and proteostasis, we screened our published transcriptomic profiles (19) for DNA sequences with unknown function that were up-regulated in conditions of enhanced protein breakdown (*e.g.*, during fasting) but not when proteolysis was blocked by FoxOs inhibition (19). Then, DNA sequences were further screened using bioinformatics tools for the presence of an Open Reading Frame (ORF) and conservation across species. To further reduce the number of candidates we searched for either the presence of the autophagy-related LIRs/GIMs (LC3 Interaction Region; GABARAP Interaction Motif) in the coding region or for published evidence of an interaction with autophagy proteins. This screening identified one candidate, *D230025D16Rik* (mouse)/*C16ORF70* (human), which we named *MYTHO* (Macroautophagy and YouTH Optimizer). This gene appeared highly conserved across species from *C. elegans* to human (37% amino acid sequence homology) and showed 95% of amino acid sequence homology between human and mouse (Supplemental Figure 1). To determine whether the *MYTHO* gene encoded a functional protein, we cloned the DNA sequence in an expression vector and transfected it into HEK293T cells. A flag-tagged 48 kDa protein was expressed in transfected cells that agrees with the predicted molecular weight of a 422 amino acid protein (Figure 1A). Quantitative RT-PCR revealed that *Mytho* is expressed in several tissues such as lung, liver, heart and in different skeletal muscles including mitochondria poor (Tibialis Anterior and Gastrocnemius) and mitochondria rich muscles (Soleus) (Figure 1B).

Since we screened for genes that may be important for longevity, we checked *Mytho* transcript expression during ageing and found an upregulation in muscles of very old mice (Figure 1C). We then checked the expression of *MYTHO* in human Vastus Lateralis muscle biopsies from patients of different age. Similar to mice, we found that the oldest group (84-96 years) displayed a significant higher *MYTHO* expression level (Figure 1D). Finally, we monitored MYTHO protein in muscle of 25-month-old mice and confirmed an increased expression (Figure 1E). To establish which nuclei of muscle tissue express *Mytho*, we consulted a published data set of single nucleus RNA sequencing from Tibialis Anterior and Soleus. Importantly, this data set contained also information of nucleus transcriptomic profiles of animals at different ages such as postnatal days 10 and 21, 5 months, 24 months and 30 months (20). When we tested which types of nuclei, among the several clusters, express *Mytho*, myonuclei showed the highest enrichment. In Soleus, the highest expression was found in myonuclei of type 2A and 2X fibers (Figure 2A, B), while in Tibialis Anterior the transcript was less abundant in adulthood but showed an age-related pattern (Figure 2C). Indeed, *Mytho* was transiently expressed in type 2X fibers at postnatal day 21 and was re-induced at 24 and 30 months of age (Figure 2D). Interestingly, also myonuclei of the neuromuscular junction (NMJ) showed a transient higher expression at postnatal day 10 and a further induction in aged animals (Figure 2D). In addition, the neuronal part of NMJ, constituted by the Schwann cells, also showed the upregulation of *Mytho* at 30 months of age (Figure 2D). These findings confirm that *Mytho* gene is regulated during neonatal life and in ageing mainly in myonuclei and nuclei belonging to the presynaptic and postsynaptic site of NMJ and to the nerve axons.

Because this gene is conserved across species and since *C. elegans* is an established animal model for ageing studies, we checked whether the *C.elegans* homologous gene *T01G9.2*, hereafter named *myt-1*, showed a similar pattern of tissue and time expression. Therefore, we generated a transgenic *C.elegans* line that expressed *gfp* coding sequence from the *myt-1* endogenous promoter (see Methods). Confocal microscopy analyses revealed that *myt-1* was mostly expressed in body wall muscles, neurons and intestine early during development (Supplemental Figure 2A), while it was mainly expressed in muscles and neurons in adulthood (Supplemental Figure 2B, C). Next, we tested *myt-1* expression in 11-day-old *C.elegans* (counting day 0 at L4 stage) and identified an increased expression in neurons and muscles compared to younger animals (3-day-old) confirming an age-related regulation also in *C.elegans*

(Supplemental Figure 2D). Finally, because the initial screening was based on genes induced when nutrients are reduced, we tested whether this expression was affected by 24 hours of starvation. Consistently, GFP signal was dramatically increased by fasting especially in body wall muscles (Supplemental Figure 2E,F). Thus, *C.elegans* replicate the mammalian tissue-pattern and age-dependent expression of *MYTHO*.

Inhibition of MYTHO induces cellular senescence and reduces lifespan in C.elegans

The finding that *MYTHO* was upregulated in very old people and mice suggested a potential role of this gene in counteracting ageing. Therefore, we tested whether inhibition of *Mytho* would induce a premature cellular senescence. To address this point, we generated a muscle cell line in which *Mytho* was deleted by CRISPR/Cas9 technology (Supplemental Figure 3A-F) and investigated cellular senescence. Premature cellular ageing is typically characterised by low replicative rates due to upregulation of cyclin inhibitors such as p21 and p16, accumulation of dysfunctional mitochondria, proteostasis dysfunction, DNA damage amongst other cellular events. In absence of *Mytho*, cell proliferation was slowed down, *p21* expression was increased, mitochondria showed abnormal morphology and function, which was revealed by ROS production, and the senescence associated β-galactosidase activity, a marker of lysosomal impairment, was increased (Figure 3 A-E). To further characterize the functional relevance of this gene in physiology as well in lifespan of a multicellular organism we moved back to *C. elegans*. By CRISPR/Cas9 technology, we generated three independent *C. elegans* mutant lines in which the *myt-1* gene was disrupted, *i.e. myt-1(pan8) I*, *myt-1(pan9) I*, and *myt-1(pan10) I* (Supplemental Figure 4A-E). Phenotypic analyses were performed on *myt-1(pan8) I* and *myt-1(pan9) I* strains. Knockout animals displayed a problem of egg delivery, as revealed by a higher prevalence of egg retention with internal hatching, called “bagging” phenotype, compared to controls (Supplemental Figure 5A), possibly due to the physiological role of *myt-1* in vulval muscles. Notably, *myt-1* animals that did not exhibit a bagging phenotype displayed a significantly shortened lifespan (Supplemental Figure 5B, Supplemental Figure 6A). Next, to better establish *myt-1* involvement in longevity independently of the bagging phenotype, we crossed the *myt-1(pan8) I* strain to *fer-15(b26) II* animals. This genetic background confers temperature-dependent sterility. Consistently, the absence of *myt-1* resulted in a dramatic

reduction of *C.elegans* lifespan (Figure 4A, Supplemental Figure 6A). Identical results were obtained by crossing a second *myt-1 (pan9) I* strain (Supplemental Figure 5C, Supplemental Figure 6A). Reduction of survival was further confirmed by RNAi mediated knockdown of *myt-1*, which significantly shortened the lifespan of *C.elegans* (Figure 4B, Supplemental Figure 6B). Moreover, when animals were challenged with oxidative stress by paraquat treatment, survival was significantly reduced compared to controls (Supplemental Figure 5D). Because lifespan does not necessary match with quality of life, we checked *C.elegans'* movements as a health readout. In fact, body movement is one of the most obvious behavioural abnormalities associated with nematode ageing (21). While the worms' movements were not significantly different in young *myt-1* knockout animals (data not shown), they were dramatically reduced in old worms (Figure 4C). Moreover, pharyngeal pumping was also significantly decreased in *myt-1* deficient old worms but not in young animals (Figure 4C, lower right panel). Importantly, a significant reduction of movement in the absence of *myt-1* was also obtained by comparing wild-type and knockout animals at the mean lifespan, supporting the role of *myt-1* in health span (Supplemental Figure 5E). These findings suggest that muscle maturation/generation was preserved during youth but that premature ageing and decline in muscle function happened in adulthood in *myt-1* deficient animals. Consistently, similar results were obtained when *myt-1* gene was knocked down by RNAi and spontaneous or touch-induced worms' movements were quantified at day 11 (Figure 4D and Supplemental Figure 5F). Next, we tested whether muscle-specific *myt-1* overexpression during ageing is beneficial for health span. We analysed the worms' movements at day 14 and found a significant increase of body bends and head movements in transgenic animals, as well as a decreased stillness time (Supplemental Figure 5G). Despite the beneficial effect on health span, lifespan was not improved (Supplemental Figure 6A). Altogether these findings strongly support that *MYTHO* is required to preserve cellular function during ageing.

MYTHO is recruited to autophagosomes and is required for optimal autophagy flux

To identify how *MYTHO* preserves cellular functions during ageing we performed localization studies in vivo and in vitro. Given the high expression level of the gene in muscles of worms and mice, and since genetic manipulation is straightforward in adult mice muscles (22), in vivo experiments were performed in skeletal muscle. Immunofluorescence analyses on transfected

HEK293 cells showed a puncta pattern of staining that was similar to the localization of the endogenous protein (Figure 5A). An identical pattern was also detected when *Mytho* was overexpressed, in adult skeletal muscles or when the endogenous protein was revealed (Figure 5B). By CRISPR/Cas12 technology (23) we HA-tagged the endogenous MYTHO protein in cells (Supplemental Figure 7A). Immunofluorescence analyses with anti-HA antibody showed a minor colocalization of MYTHO with mitochondria and peroxisomes, and almost no co-localization with endoplasmic reticulum (ER) or Golgi in basal conditions (Supplemental Figure 7B-F). Interestingly, we found that 40% of DFCP1-positive puncta, which under starvation conditions reveal the ER regions enriched of phosphatidyl-inositol 3-Phosphate (PtdIns3P) named omegasomes, colocalized with MYTHO (Supplemental Figure G). Because of this finding and since the initial bioinformatic screen suggested several putative LC3B interaction regions (LIR) in the protein, we tested whether MYTHO colocalized with LC3B or LAMP2, two established markers of autophagosomes and lysosomes, respectively. MYTHO-GFP colocalized with Cherry-LC3B (Supplemental Figure 8A), in vitro, and with LAMP2-Cherry, in vivo (Supplemental Figure 8B). Moreover, when we expressed MYTHO-GFP in muscle-specific autophagy deficient *Atg7* knockout mice, MYTHO localization on lysosomes was completely abrogated suggesting that it requires autophagy to reach lysosomes (Supplemental Figure 8B). Finally, by pulling down with anti-HA antibody the endogenous tagged MYTHO protein we confirmed that LC3B II co-immunoprecipitates (Figure 5C). To further support the critical role of MYTHO in autophagy we tested the autophagic flux in a Mytho knockout C2C12 cell line (Figure 5D) by monitoring the increase of LC3II in presence of chloroquine, a lysosome inhibitor. Indeed, the accumulation of the lipidated LC3 (LC3II) protein during lysosomal inhibition is proportional to the number of autophagosomes that are generated and docked to the lysosomes. Western blots for LC3 lipidation and immunofluorescence analyses of LC3-positive puncta revealed that chloroquine treatment did not increase LC3-II lipidation in Mytho knockout cells as in control cells indicating that basal autophagy flux is reduced in absence of Mytho (Figure 5D, E). Consistently, the number and size of p62 positive puncta were significantly increased in *Mytho* deficient cells (Supplemental Figure 8C). Finally, when we crossed knockout *myt-1* nematodes with animals expressing a GFP-tagged version of LGG-1 (the worm orthologue of ATG8/GABARAP), we noticed a significant decrease in the number of LGG-1 puncta localized at the posterior bulb of pharynx in knockout animals compared to wild-type, suggesting

that *myt-1* is required for autophagy also in *C. elegans* (Figure 5F). To further support *myt*-1 involvement in autophagic flux regulation in vivo, we crossed *myt-1* knockout worms with nematodes expressing the tandem reporter mCherry::GFP::LGG-1 and quantified red puncta in pharynx and body wall muscles. Because green fluorescence was blunted by the acidic environment of lysosomes, the red signal revealed the number of autophagosomes fused with lysosomes. Consistent with cell culture data, red puncta were significantly decreased in pharynx and muscles from *myt-1* deficient worms upon starvation (Figure 5G-H) suggesting that autophagic flux is reduced also in *C. elegans*. Conversely, overexpression of *Mytho* in adult mice skeletal muscles was sufficient to increase autophagosome numbers (Figure 5I). These findings suggest that *Mytho* is involved in autophagosome formation both in vitro and in vivo.

MYTHO interacts with WIPI2 allowing the recruitment of the conjugation system at the phagophore.

To identify how *Mytho* controls autophagy we pulled down MYTHO and performed proteomic analyses to establish its interactome. Among the different interactors, WIPI2, which plays a critical role in autophagy, as well as different autophagy receptors (*e.g.*, p62/SQSTM1, NCOA) were identified (Figure 6A). Interestingly, another PtdIns3P binding protein, BCAS3, that has been described to be involved in autophagosome formation (24) was enriched in MYTHO pulldown experiments. We found that WIPI2 puncta were dramatically reduced in starved *Mytho*-deficient cells (Figure 6B, Supplemental Figure 9A) even though total WIPI2 protein was not affected (Supplemental Figure 9B). Accordingly, the recruitment and colocalization of ATG16L1, another WIPI2 partner, with WIPI2 was abolished (Supplemental Figure 9C). Interestingly, BCAS3 puncta were also abolished in absence of MYTHO during starvation (Supplemental Figure 9D). Furthermore, endogenous MYTHO could be co-immunoprecipitated with GFP-WIPI2 together with BCAS3 (Figure 6C, Supplemental Figure 9E). Moreover, immunoprecipitation of MYTHO-GFP showed an interaction with endogenous WIPI2, BCAS3 and ATG7, the E1 enzyme of the conjugation system, but not BECN1, the protein involved in PtdIns3P generation (Figure 6D, Supplemental Figure 9F). Immunofluorescence analyses with anti-HA antibody for the endogenous HA-tagged MYTHO protein highlighted the co-localization with WIPI2 and ATG16L1 (Supplemental Figure 10A).

To identify the regions of interaction with LC3 and WIPI2 we mutagenized the putative LIR or WD40 domains of MYTHO (Figure 7A) and performed immunoprecipitation experiments. By pulling down the different MYTHO mutants we found that the interaction with lipidated LC3B was abolished when motif 1 (M1) was mutated (Figure 7B, Supplemental Figure 10B). Interestingly, when we checked for the presence of WIPI2 in MYTHO immunoprecipitated complex, we showed a reduction of WIPI2 binding to MYTHO when motif 3 (M3) and 4 (M4) were altered, and a slight reduction with mutated M1 (Figure 7B, Supplemental Figure 10C). BCAS3 interaction was also lost by altering these motifs M3 and M4 (Figure 7B, Supplemental Figure 10D). Since the mutagenesis of M3 disrupted one putative WD40 out of two, we also mutagenized this second site (M5), and both M3/M5 motifs and found a reduction of WIPI2 as well as ATG16L1 binding and the absence of BCAS3 interaction (Figure 7C). Thus, M1 is important for LC3B interaction while M3 and M4/5 modulate WIPI2 interaction. To establish whether the MYTHO-WIPI2 interaction occurs on the PtdIns(3)P enriched membrane we expressed in cells the WIPI2 mutant (WIPI2-FTTG), which is unable to bind PtdIns(3)P, for pull down experiments. Interestingly, the WIPI2-FTTG/MYTHO complex was preserved suggesting that this interaction happened independently of WIPI2 recruitment at the PtdIns(3)P enriched membranes (Figure 7D). Next, we asked whether the interaction of MYTHO with WIPI2 depends on the ability of WIPI2 to bind ATG16L. By pulling down the WIPI2-RERE mutant, which is unable to bind to ATG16L1, we could not detect endogenous MYTHO (Figure 7D). Thus, MYTHO binds the WIPI2-ATG16L complex independently of the recruitment of WIPI2 to the PtdIns(3)P enriched membranes.

To further support the direct role of MYTHO in the recruitment of WIPI2 complex to the phagophore we restored MYTHO protein in knockout cells and found that WIPI2 puncta were re-established in absence of nutrients (Figure 7E). Consistently, the rescue of MYTHO protein in knockout cells restored the levels of LC3 positive puncta (Figure 7F). Finally, when we expressed the M1 and M3 mutants, which showed a reduced LC3 and WIPI2 binding respectively, WIPI2 puncta were restored by M1 expression (Figure 7G) while LC3-puncta were not rescued by any of the mutants (Figure 7F). Consistently, expression of mutants M5 or M3/5 did not rescue WIPI2 puncta (Figure 7G, Supplemental Figure 10E). Altogether, MYTHO plays a fundamental role in WIPI2 recruitment at the phagophore site and in autophagosome formation.

MYTHO acts in different longevity pathways.

Since *myt-1* inhibition reduced worm survival, we investigated if *myt-1* is required in any longevity pathway by genetic interaction experiments. Loss-of-function mutations in the insulin receptor *daf-2* increase lifespan through the activation and translocation to the nucleus of the transcription factor *daf-16*/FOXO (2, 4). To establish whether *myt-1* mediates the Insulin-dependent effect on longevity, we crossed *daf-2(e1370) III* animals with *myt-1*-deficient worms and checked lifespan. Importantly, *myt-1* ablation did not suppress the extended lifespan of *daf-2(e1370) III* mutants, thus is not required for *daf-2* mediated longevity (Figure 8A, Supplemental Figure 6A). Similar results were obtained when *daf-2* was knocked down in adult *myt-1* mutants (Supplemental Figure 11A, Supplemental Figure 6B). Next, we used a pharyngeal pumping defective *eat-2* mutant (namely *eat-2(ad1116) II*), which mimics caloric restriction due to its reduced food intake, leading to extended lifespan (25). Ablation of *myt-1* significantly reduced the longevity of *eat-2(ad1116)* mutants suggesting that it was partially indispensable for lifespan extension due to dietary restriction (Figure 8B, Supplemental Figure 6A) but with a smaller effect size compared to its effect on WT worms, as confirmed by Cox proportional hazards (CPH) analysis (P=0.00004). The Notch family receptor *glp-1* mediates Notch signaling and controls the mitotic proliferation of germline cells (26, 27). The g*lp-1(e2141) III* strain carries a *glp-1* loss-of function mutation and shows prolonged lifespan when maintained at the non-permissive temperature due to failed germline proliferation (28). Importantly, lifespan extension of the g*lp-1(e2141)* mutant was completely abolished when crossed with *myt-1* mutants, suggesting a critical function of this gene in the longevity pathways activated by *glp-1* deletion (Figure 8C, Supplemental Figure 6A). Similar results were obtained by knocking down *glp-1* in *myt-1* mutants (Supplemental Figure 11B, Supplemental Figure 6B). Altogether, these results indicate that *myt-1* is required for *glp-1* mediated lifespan and partially indispensable for *eat-2* mediated longevity.

Finally, we explored the involvement of MYTHO in the autophagy-mediated effects on lifespan and specifically on the WIPI2 pathway and BECN1 signalling. Our findings showed that MYTHO interacted with WIPI2 but not with BECN1. We knocked down *atg-18* or *bec-1*, the nematode homologs of human *WIPI2* and *BECN1* genes respectively, in wild-type and *myt-1* KO

worms and measured their survival. Knock down of *atg-18* resulted in a decreased lifespan of control and *myt-1* KO animals. Interestingly, the reduction in lifespan was less evident in the *myt-1* mutant background (Figure 8D, Supplemental Figure 6B). CPH analysis showed a statistically significant interaction between *myt-1* deletion and *atg-18* knockdown ($P<0.0001$) supporting an epistatic link between ATG-18 and MYT-1. Besides their influence on worm lifespan, the epistatic interaction between MYTHO and WIPI2 was further supported by other analysis. Indeed, the improved locomotion activity induced by *myt-1* overexpression in muscles (*fer-15(b26) II; oxTi0882; syls321)* was blunted when *atg-18* was knocked-down (Figure 8F). Interestingly, knocking down *bec-1* did not affect the survival curves of *myt-1* KO worms in a significant manner, while having a minor effect on extending WT worms longevity (Figure 8E, Supplemental Figure 6B). However, CPH analysis between *bec-1* knockdown and *myt-1* deletion suggested a minor but significant epistatic interaction between BEC-1 and MYTHO ($P=0.015$). To verify *bec-1* silencing efficiency, we fed worms that expressed a GFP-tagged version of BEC-1 (FR758 strain) with bacteria expressing dsRNA for *bec-1* (see Supplemental Figure 11C and Methods section for strain details), and noticed a clear reduction of GFP signal compared to controls. Moreover, long-lived *eat-2(ad1116)* mutants when fed with bacteria expressing dsRNA *bec-1* showed a decrease of lifespan (Supplemental Figure 11D, Supplemental Figure 6B), as previously reported (29). Overall, these data are consistent with *myt-1* being downstream of WIPI2/ATG-18 pathway.

In conclusion, we characterized the function of an uncharacterised gene that is fundamental for lifespan and healthspan being involved in WIPI2 recruitment at the phagophore site and in autophagosome formation.

DISCUSSION

The identification of genes that confer either extension of lifespan or accelerate age-related decline has been a step forward in our understanding the mechanisms of senescence and revealed that the ageing process is partially controlled by genetics. However, this genetic contribution is only partially understood, likely because many genes are not yet clearly characterized for their possible role in maintenance and repair processes ensuring short or long lifespans. To investigate the role of *myt-1* in pro-longevity interventions we tested the long-lived *glp-1(e2141) III* (which

shows reduced proliferation of germline cells) and *eat-2(ad1116) II* (a genetic dietary restriction model) mutants. The findings that the absence of *myt-1* completely blunted the life extension of *glp-1* mutants and partially affected the longevity of *eat-2* mutants suggest that *myt-1* is mediating the response to germline signals and dietary cues, respectively (see Figure 8 legend for Cox-proportional hazards analysis of interaction of terms *myt-1* and other genotypes). Thus, *myt-1* is required for both natural longevity and in specific pro-longevity interventions.

Mechanistically, we found that MYTHO/*myt-1* played a critical role in autophagy regulation and particularly, in WIPI2-ATG16L and ATG7 recruitment on the phagophore under stress conditions. Consistent with this hypothesis, MYTHO localized at DFCP1 positive sites. Moreover, *Mytho* deficient cells showed a significant reduction of WIPI2 positive puncta and autophagosome formation upon nutrient deprivation. The interactome as well as immunoprecipitation and rescue experiments confirmed that MYTHO binds WIPI2-ATG16L complex via the WD40 domains. Our findings are supported by two other independent studies in which MYTHO was found in the interactome of the autophagy protein WIPI2/Atg18 (30, 31). WIPI2 functions as a PtdIns3P effector bridging PtdIns3P production with the recruitment of the ATG5-ATG12-ATG16L complex to permit the covalent binding of LC3B/ATG8 to the phospholipid, phosphatidylethanolamine (lipidation reaction) (32). When we mutagenized WIPI2 to hinder its binding to PtdIns3P, we still detected the interaction with MYTHO suggesting that the complex is formed independently of the recruitment on PtdIns3P enriched membranes. Importantly, this interaction was disrupted when WIPI2 was mutagenized in the domain for ATG16L binding, suggesting that MYTHO binding happens only when the complex WIPI2-ATG16L is formed. Because *Mytho* ablation did not completely suppress autophagy as well as ATG16L puncta, other mechanisms for the conjugation system recruitment also exist and synergize with MYTHO/WIPI2 complex to maximally activate the E3 enzyme and the lipidation process (33). For instance, ATG16L has been reported to bind the ATG1/ULK1 complex via FIP200 (34) (35), and directly to PtdIns3P enriched membranes (33, 36, 37). However, the striking phenotype of worms and the effect on mitochondria, cellular senescence and oxidative stress underline the important physiological function of *MYTHO*. Since mutations of *WIPI2* caused multi-organs defects in humans with a premature ageing phenotype (38), it will be interesting to explore whether mutations of *MYTHO* also cause disease onset in humans. Interestingly, *MYTHO* has been reported to be fused in frame with *ABCC6* and *ARL16* genes in

acute myeloid leukemia and lung squamous cell carcinoma, but the pathogenetic role of the fused transcripts has not yet been explored (39). Consistently, we recently found that when *Mytho* expression was inhibited chronically it resulted in muscle degeneration and myopathy (40). Some of the myopathic features differ from the ones that characterize autophagy failure, suggesting that *MYTHO* is involved in other cellular biological processes that are critical for cell survival. This hypothesis is also supported by the finding that *myt-1* ablation did not shorten the lifespan of the long lived *daf-2(e1370)* while the autophagy genes are required for the life span extension of this mutant (11, 12). This discrepancy suggests that *myt-1* could be involved in other longevity-related functions that are autophagy-independent and that will be investigated in future studies.

METHODS

Additional methods are provided in the Supplemental Methods.

Plasmid cloning

Murine *Mytho* coding sequence (1239bp) was amplified by cDNA obtained from skeletal muscles of tumour-bearing mice and cloned in p3XFlag-Myc-CMV vector (6.4Kb) (Addgene, Watertown, MA, USA) using KOD Hot Start DNA polymerase (Merck Millipore, Darmstadt, Germany) and the following primers with sticky ends: Fw 5'-AAAGATCTACTGGACCTGGAGGTGGT -3', Rw compl. 5'-TTTGATATCTTAGGGCAGCTCTGCTGTTCT -3'. Vector and insert were digested using the restriction enzymes BglII and EcorV with buffer 3 (New England Biolabs, Ipswich, MA, USA) at 37 °C for 2h and digested vector and insert were purified after having excised bands from 1% agarose gel with PCR gel DNA clean (Merck Millipore).

Mytho gene was also subcloned in pEGFP-N3 vector (4.7 kb) (Addgene) with KOD Hot Start DNA polymerase (Merck Millipore) using the following primers with sticky ends: Fw 5'-AAAGCTAGCATGCTGGACCTGGAGGTGGT-3', Rw compl 5'- TAAGGATCCGGGCA GCTCTGCTGTTC -3'.

To monitor LC3II puncta we also subcloned *Mytho* in a PBI3xFlag vector that contains YFP-LC3 expression gene in a different cloning site (PBI YFPLC3-3xFlagMYTHO, Addgene) using KOD Hot Start DNA polymerase (Merck Millipore). We designed the following primers with sticky ends: Fw 5'- AAAGCTAGCATGCTGGACCTGGAGGTGGT 3', Rw compl. 5'-GGTGATATCTTAGGGCAGCTCTGCTGTTCTCA -3'. Vector PBI and insert were digested using the restriction enzymes NheI-HF and EcorV-HF (New England Biolabs) at 37 °C for 2h and digested vector and insert were purified after having excised bands from 1% agarose gel with using PCR gel DNA clean (Merck Millipore). 50ng of vector with 3-fold molar excess of insert were ligated using the Quick ligation kit (New England Biolabs).

To generate stable cell lines, *MYTHO* cDNA was cloned into pDONR223 vector (Addgene) by using the BP Clonase Reaction Kit (ThermoFisher Scientific, Watham, MA, USA) and further recombined into the lentiviral GATEWAY destination vector pLenti-UBC-gate-3xHA-pGK-PUR (#107393, AddGene).

Other plasmids used in this project were: Cherry-LC3B, LAMP2-Cherry, Golgi-GFP, GFP-WIPI2, ATG16L1-Flag, GFP-WIPI2b RERE (R108E/R128E) mutant and GFP-WIPI2b FTTG mutant provided by our collaborators Prof. Tooze(32).

C. elegans strains, growth conditions and maintenance

The strains Bristol N2 (wild-type), DH26 (*fer-15(b26) II*), DA2123 (*lgg-1p::GFP::lgg-1+rol-6(su1006)),* MAH215 (*sqIs11* [*lgg-1p::mCherry::GFP::lgg-1 + rol-6*]), DA1116 (*eat-2(ad1116) II*), CB4037 (*glp-1(e2141) III)*, CB1370 (*daf-2(e1370) III*) were obtained from the *Caenorhabditis* Genetics Center (University of Minnesota, MN, USA). FR758 strain (*swEx520[pbec1::BEC-1::GFP + rol-6(su1006)]*) was a kind gift of Prof. Tibor Vellai (Department of Genetics, Eötvös Loránd University, Budapest, Hungary (1117 Budapest, Pázmány Péter stny. 1/C) Strains were grown on nematode growth media (NGM) agar plates at 20 °C (or 25 °C where indicated), seeded with *E. coli* OP50 (or HT115(DE3)) bacteria and genetic crosses were performed as described. When indicated, age of worms refers to specific larval stage L4, young adult stage, or reproductive adults, starting to count from day 1 of adulthood.

Genome editing in _C. elegans_

Generation of *myt-1(pan8) I* and *myt-1(pan9) I* strains

The human gene *MYTHO* has one orthologue in *C. elegans*, that is *T01G9.2* (hereafter renamed *myt-1*), which displays two isoforms (a, NM_171841.9 and b, NM_059851.6) differing of the three amino acids KFK, from position 21 to 23, that are present only in isoform a.

Genetic ablation of *myt-1* was obtained using CRISPR/Cas9 technology with a modified protocol (41). Briefly, twenty wild-type animals were injected with a mix containing 750 ng/µl Cas9 (Integrated DNA Technologies, Inc., IDT, Coralville, IA, USA), 700 ng/µl ALT-R CRISPR tracrRNA (IDT), 115 ng/µl dpy-10 crRNA, 37.5 ng/µl ssODN dpy-10, 400 ng/µl *T01G9.2* crRNA (5'-TGAAGAAGATCTGAGCTTCA -3') and 175 ng/µl of the *T01G9.2* KO ssODN (5'-CATCGAAAATGAATGGCAAACAGCAAGTTACAAAATAACCGTCGACTGAGGAAGAC CTAAGCTTCACGTTTGTTTTAAAGTCAAAAAATCAATAATAA -3'), recovered in M9 buffer and incubated at 20 °C. Animals with roller or dumpy phenotypes were isolated, as well as pools of 5 wild-type worms from those plates. To isolate mutant animals, PCR amplification

was performed using a single forward primer (5'-TGAAAAGTCGATAAAAATTCAGTAGCA -3') and two reverse primers annealing specifically with the mutated (5'-CTCAGTCGACGGTTATTTTGTA -3') or the wild-type sequence (5'-ACCTTTTTACTGTACTTCAATTCGACT -3'). Homozygosity was confirmed by Sanger sequencing using standard techniques. Four null strains were generated. Three of them carried a frameshift mutation predicted to lead to the formation of a premature stop codon at position 36, *i.e.*, *T01G9.2*(*pan8*[S18Tfs*19]); *T01G9.2*(*pan9*[S18Tfs*19]); *T01G9.2*(*pan10*[S18Tfs*19]). Independent strains *T01G9.2*(*pan8*[S18Tfs*19]) and *T01G9.2*(*pan9*[S18Tfs*19]), renamed *myt-1(pan8) I* and *myt-1(pan9) I*, were outcrossed twice to remove possible off-target mutations, and used for phenotypic analyses. In particular, experiments were performed using the *myt-1(pan8) I* strain and some results were confirmed on *myt-1(pan9) I.*

Generation of a *myt-1* translational GFP reporter strain

The *issEx1 [myt-1p::gfp]* transgenic line was obtained as described in (42). Briefly, 501 and 864 bp of 5'UTR immediately upstream of *myt-1* first ATG codon were tested as putative promoter regions. Both sequences were amplified from worm genomic DNA using a Rw primer that contains a 24-nucleotide overlap to the *gfp* sequence. In parallel, the coding sequence of *gfp* and the 3'UTR of the *unc-54* gene were amplified from pPD95.75 vector (Fire kit, Addgene). The two amplicons were then fused by PCR and the correctness of the final product was checked by agarose gel. 5 fusion-PCR products were pulled together and injected in the gonads of young adult N2 worms. GFP+ worms were observed only with the fusion product containing the longer *myt-1* 5'UTR. These were then selected and isolated to verify transgene transmission in the progeny. Three independent lines were generated and used to analyze *myt-1* expression.

Generation of a body wall muscle *myt-1* overexpressing line

We purchased from the Genome Engineering Facility of the Max Planck Institute of Molecular Cell Biology and Genetics (Dresden, Germany) the body wall muscle driver strain PS6936 (*syIs321 [myo-3p::NLS::GAL4SK::VP64::unc-54 3'UTR + myo-2p::NLS::mCherry + pBlueScript]*) that expresses a mCherry reporter in the pharyngeal muscles (43) and the effector strain *oxTi10882 [15xUAS-T01G9.2a-SL2-mScarlet-glh-2_3'UTR],* carrying a transgene inserted in chromosome IV consisting of *myt-1* coding sequence (isoform a) downstream the UAS

element with mScarlet reporter. Progeny resulting from the cross of driver and effector strain is recognizable by the mScarlet fluorescence in body wall muscles. Then, *oxTi10882; syIs321* worms were crossed with DH26 *(fer-15(b26) II))* animals, that have a temperature-sensitive defect in spermatogenesis and are thus sterile at 25 °C, in order to obtain *fer-15(b26) II; oxTi10882; syIs321* worms. Two independent lines were generated and used in the experiments.

Generation of *Mytho* knockout C2C12 cell line using CRISPR/Cas9

C2C12 cell line was purchased from ATCC (Manassas, VA, USA) and cells were grown in Dulbecco's Modified Eagle Medium (DMEM) supplemented with 10% Fetal Bovine Serum (FBS, scomplemented at 55 °C for 1 h,), 1% Penicillin/Streptomycin and 1% L-Glutamine (reagents for cell cultures were purchased from Gibco, ThermoFisher Scientific).

To generate the *Mytho* KO C2C12 line, cells were co-transfected with Transedit CRISPR all-in-one lentiviral expression vectors (pCLIP-ALL-EFS-Puro) containing two different CRISPR target sequences of murine *Mytho* (TEVM-1183975 and TEVM-1251117, Transomic Technologies, Huntsville, AL, USA), targeting exon 1 and exon 2, respectively. Transfections were performed using Lipofectamine® 2000 (ThermoFisher Scientific), according to the manufacturer's protocol.

After 24h cells were selected by the addition of puromycin (Gibco, ThermoFisher Scientific) at 1 µg/ml to the culture medium until the untransfected control cells were all dead. To isolate single clones, cells were serially diluted and seeded in 96-well plates. After growth and expansion of clones, genomic DNA was extracted from cells using standard protocols and fragments encompassing the CRISPR target sequences were amplified by PCR. Two different PCR reactions were performed, the first with two primers upstream and downstream the first guideRNA target (Fw primer 5′- CCACTTTTGCTGCAGTTGCT -3′ and Rw primer 5′- TGCTGAGACATCGCTGATCC -3′) and the second with the same forward primer and as reverse an oligonucleotide downstream the second guideRNA target (5′- TGAAAAGGCCCCCATGTGAA -3′). PCR reactions were then sequenced and 4 different clones harbouring truncating mutations were mixed to reduce the consequences of possible CRISPR/Cas9-mediated off-target effects.

Endogenous HA tagging of MYTHO in HeLa cells using CRISPR/Cas12

HeLa cells were purchased from ATCC (Manassas, VA, USA) and grown in Dulbecco's Modified Eagle Medium (DMEM) supplemented with 10% Fetal Bovine Serum (FBS), 1% Penicillin/Streptomycin and 1% L-Glutamine (reagents for cell cultures were purchased from Gibco, ThermoFisher Scientific). Cells were constantly monitored for mycoplasma contamination. To generate the endogenous HA tag at the C-terminal region of Mytho, we used the protocol described in (23). Briefly, oligos were designed by using www.pcr-tagging.com to generate the PCR cassette: M1_Mytho:5'-
CACCAGGTCATGCAGAACAACCACATTGCCTCGGTGACCCTGTATGGCCCCCCCAGG
CCTGGTAGCCACCTGAGAACAGCGGAACTCCCCTCAGGTGGAGGAGGTAGTG -3'
M2_Mytho_LbCpf1_TYCV:5'-
GAGCAGGATGTGATGCACAGTTCCACGGGACAGAGGGGCATGGGTGGTGGTGTCCA
AAAAAATGGGTGGTGGTGTCCCTAGATCTACACTTAGTAGAAATTAGCTAGCTGCAT
CGGTACC -'3
As template of the PCR cassette, plasmid pMaCTag-P27(1X HA) (Addgene) was used. Cells were transfected with PCR cassette and Cas12 plasmid pcDNA3.1-hLbCpf1(TYCV)(pY230) (Addgene) using Lipofectamine® 2000 (ThermoFisher Scientific).
48h post-transfection, cells were selected by the addition of puromycin at a concentration of 2 µg/mL over a period of 2 weeks. To exclude not-specific tagging, cells were tested by genomic extraction followed by a PCR amplification of segments targeting the predicted integration of HA at Mytho C-terminal region. PCR products were analysed by gel electrophoresis. In addition, the integration was also verified by WB testing cell lysates with anti-HA antibody (#3724, Cell signalling Technology Inc., Danvers, MA, USA).

Generation and propagation of HA-MYTHO stable and inducible cell lines

Stable cell lines were produced using lentiviral virus infection. Viruses were produced using HEK293T cells, purchased from ATCC (Manassas, VA, USA). HeLa stable cell lines were generated cloning the cDNAs into pLenti-UBC-gate-3xHA-pGK-PUR lentiviral vector carrying an 3xHA tag at the C-Terminal (#107393, Addgene).

Immunofluorescence analysis

Cells were fixed in 4% paraformaldehyde in PBS for 10 minutes, permeabilized with 0.3% Triton X-100 in PBS for 2 minutes and then blocked using 0.5% bovine serum albumin (BSA), 10% goat serum in PBS. Slides were incubated for 24h at 4 °C with primary antibodies (1:100) and after 3 washes with secondary antibodies (1:200) for 1h at room temperature. Nuclei were stained with Hoescht and mounted with fluorescent mounting medium (Dako Omnis, Agilent, Santa Clara, CA, USA). The following primary antibodies were used: anti-flag M2 (#F3165, Sigma Aldrich-Merck, Darmstadt, Germany), anti-C16orf70 (#ab181987, Abcam, Cambridge, UK), anti-WIPI2 antibody (purified mouse IgG clone 2A2 from the Tooze lab), anti-HA (#H3663, Sigma Aldrich-Merck), anti-VDAC (#D73D12, Cell signalling Technology Inc.), anti-PDI (#C81H6, Cell Signalling Technology Inc.), anti-PMP70 (#P0497, Cell Signalling Technology Inc.), Anti-BCAS3 (#ab71162, Abcam). Secondary antibodies were: Alexa Fluor anti-rabbit or anti-mouse cy3, 647 or 488 (Jackson Immunoresearch, Cambridgeshire, UK).

Immunoblotting

Forty Tibialis anterior (TA) cryosections of 20 µm thickness were lysed in 100 µL of lysis buffer (50 mM Tris pH 7.5, 150 mM NaCl, 10mM $MgCl_2$, 0.5 mM DTT, 0.5 mM EDTA, 10% glycerol, 2% SDS, 1% Triton X-100), protease inhibitor cocktail and phosphatase inhibitors cocktail I and II (Roche, Basel, Switzerland). Protein quantification was determined by BCA kit (Pierce, ThermoFisher Scientific).

C2C12 myoblasts or HEK293 cells were washed and lysed with 100 µL RIPA buffer supplemented with protease inhibitors and phosphatase inhibitors (Roche). Cells were incubated in lysis buffer on ice before being scraped and transferred into a clean Eppendorf tube. After 15 minutes of centrifugation at 15000 g, the supernatant was collected for quantification with BCA kit (Pierce).

30 µg of muscle protein lysate and 10 µg or 20 µg of cell lysate were loaded on SDS-PAGE gel (ThermoFisher Scientific) and electroblotted into a Nitrocellulose membrane. Transfer buffer (Bio-Rad Laboratories S.r.l., Hercules, CA, USA) was prepared as following: 10x Tris-glycine, 20% methanol in H_2O. Membranes were saturated with blocking buffer (5% non-fat milk powder solubilized in TBS 1x with 0.1% Tween).

The following antibodies were used: anti-GAPDH (#32233, Santa Cruz Biotechnology, Inc., Dallas, TX, USA), rabbit anti-Flag(#F7425, Sigma Aldrich-Merck) or M2 (#F3165,Sigma

Aldrich-Merck), anti-LC3B (#L7543, Sigma Aldrich-Merck), anti-WIPI2 (purified mouse IgG clone 2A2 from the Tooze lab), anti-GFP (#A11122, ThermoFisher Scientific), anti-C16orf70 (#ab181987, Abcam), anti-ATG16L1 (#D6D5, Cell Signalling Technology Inc.), anti-Beclin 1 (#D40C5, Cell Signalling Technology Inc.), anti-ATG7 (#D12B11 Cell Signalling Technology Inc.), anti-HA (# C29F4, Cell Signalling Technology Inc.), anti-BCAS3 (#ab71162, Abcam).

MYTHO site-directed mutagenesis

LIR or WD40 domains were identified by using http://ilir.uk/model/search.php (44) and http://elm.eu.org/ (45) databases. Site-directed mutagenesis of some motifs in MYTHO-GFP plasmid was performed by using Q5-site directed mutagenesis kit (New England Biolabs) according to the manufacturer's instructions. The following primers were designed to mutagenize the crucial amino acids: Mutation Motif region1 (M1) Y91A/V94A Fw 5'-AAAGTAAAGTTAAAGGCTTGTGGAGCTCATTTTAACTCTCAGGCC -3' Mutation Motif region2 (M2) F131A/L134A Fw 5'- CTCTTCCACCTCAACGCTCGAGGAGCT TCTTTCTCTTTTCAG -3' Mutation Motif region3 (M3) Y288A/L291A Fw 5'-GACTACTTTTTTAACGCTTTTACTGCTGGAGTGGACATCCTG -3' Mutation Motif region 4 (M4) Fw W351A/I354A 5' - ACAACCTACAGCAAGGCTGACAGCGCTCAGGAGCTTCTG -3'; Deletion of Motif region 5 (M5) 208delTGPSGLRLRL Fw 5'- CGCTTGCTCGCTGCAGGTTGTGGA -3' and Rw compl 5'- TCCATCTCGAAGAACGTCTACACTTTCAGCA -3'; Mutation Motif region 3 and 5 (both WD40 regions) M3/M5: Y288A/L291A + 208delTGPSGLRLRL using the primers described above. PCR conditions for gene amplification were: 98 ºC for 30 sec, then 25 cycles at 98 ºC 10 seconds, 72 ºC 30 sec and 72 ºC 2.5min; final extension at 72 ºC for 2 min. After PCR, the product is incubated with the Kinase-ligase-DpnI (KLD) enzyme mix (New England Biolabs) for 5 minutes at room temperature for rapid circularization and template removal. Transformation was performed using the high efficiency NEB® 5-alpha Competent *E. coli* (New England Biolabs).

Immunoprecipitation

$3x10^6$ cells were seeded into 10-cm dishes for Lipofectamine® 2000 (ThermoFisher Scientific) transfection. 24 hours after transfection cells were lysed using 1000 µl of TNTE lysis buffer (20

mM Tris-HCl pH 7.4, 150 mM NaCl, 5 mM EDTA and 0.3% Triton X-100) supplemented with 1x PhosSTOP (Roche) and 1x EDTA free Complete Protease Inhibitor Cocktail (Roche). After the lysis, cells were centrifuged at 13000 rpm for 10 minutes at 4 °C and 10ul of supernatant was used as 1% input for western blot analysis. The remaining sample was immunoprecipitated using 10 uL of GFP-TRAP beads from iST GFP-trap kit (ChromoTek, Proteintech Group, Inc., Rosemont, IL, USA). GFP beads were washed four times with buffer TNTE before immunoprecipitation. Lysate was incubated with GFP-TRAP beads for 2-3 hours, rotating at 4 °C. Then beads were centrifugated and 0.5% or 1% of the unbound fraction was taken for immunoblot analysis. All immunoprecipitation samples were washed four times with TNTE buffer before adding 30µl of 2x SDS sample buffer and boiling for 5 minutes at 100 °C. After centrifugation of the beads, 20 µl of the supernatant were loaded for immunoblot analysis.

Lifespan analysis

Experiments with mutant lines

Lifespan of *myt-1(pan8) I* and *myt-1(pan9) I* worms was firstly assessed compared to Bristol N2 animals. Moreover, *myt-1(pan8) I, myt-1(pan9) I, daf-2(e1370) III*, *eat-2(ad1116) II* and *glp-1(e2141) III* worms were crossed with *fer-15(b26) II* animals. *myt-1(pan8) I; fer-15(b26) II* were then crossed with *eat-2(ad1116) II, glp-1(e2141) III,* or *daf-2 (e1370) III* strains in order to obtain *myt-1(pan8) I; myt-1(pan8) I; fer-15(b26) II, daf-2(e1370) III, myt-1(pan8) I; fer-15(b26) II; eat-2(ad1116) II , myt-1(pan8) I; fer-15(b26) II; glp-1(e2141) III* worms.

RNAi experiments

myt-1 coding sequence (which included both isoforms) was cloned into pL4440 empty vector (Fire Kit, Addgene) (*myt-1(RNAi)*), *atg-18* RNAi clone (V-14D09) was purchased from Source BioScience (Nottingham, UK) and *bec-1* RNAi clone was a kind gift of Prof. Julián Cerón Madrigal (Modeling human diseases in C. elegans Group; Genes, Disease and Therapy Program, Institut d'Investigació Biomèdica de Bellvitge - IDIBELL, L'Hospitalet de Llobregat, 08908, Barcelona, Spain). Plasmids pAD48-*daf-2* RNAi (Addgene plasmid # 34834; http://n2t.net/addgene:34834; RRID:Addgene_34834) and pAD12 (Addgene plasmid # 34832; http://n2t.net/addgene:34832; RRID:Addgene_34832) were a gift from Cynthia Kenyon (Department of Biochemistry and Biophysics, University of California, San Francisco, San

Francisco, California 94158, USA) (46). HT115(DE3) bacteria, transformed with each RNAi construct, were seeded on NGM plates containing 1mM isopropyl- ß-D-thiogalactopyranoside (IPTG) and 100 µg/mL carbenicillin (RNAi plates). For each RNAi experiments, a positive control, obtained feeding worms with bacteria carrying the pLT61 vector (Fire Kit, Addgene), was included. This plasmid contains 0.8 kb of *unc-22*, a gene whose silencing causes a visible shaking phenotype, inserted into the pL4440 vector.

RNAi was performed following two different protocols. For maternal RNAi treatment *fer-15*(*b26*) *II* worms were allowed to grow until L4 on NGM plates seeded with OP50 at 16 °C and then transferred to RNAi plates for two days at 20 °C. Progeny was then transferred at L4 stage to a new RNAi plate for the beginning of longevity experiment. For adulthood RNAi treatment, *fer-15*(*b26*) *II* worms were seeded on NGM plates seeded with OP50 and left to grow until L4/young adult stage. Then animals were transferred to RNAi plates for lifespan experiment.

Lifespan with mutant lines and RNAi treated worms was performed as previously reported(47) at 20 °C (background N2) or 25 °C (background *fer-15(b26) II*). Animals were scored every day and counted as dead if they did not move after repeated stimuli with platinum wire, while those that crawled off the plate, had extruded organs or showed hatched progeny inside the uterus ("bag of worms" or "bagging"), were censured. Bagging was observed only in experiments performed at 20 °C in N2 background. Survival curves, which represent the composite of at least two independent experiments performed, were compared using the log-rank test.

Worm movement analysis

Worms were individually transferred on NGM plates seeded with OP50 bacteria at the L4 stage and maintained at 25 °C until the experiment (see graphs/figure legends for details about timing and genotypes analysed). Spontaneous locomotion was observed and measured for 30 seconds in two separate intervals and for each worm the total number of body and head bends, reversals and duration of stillness periods was calculated as reported(48, 49). Analysis was also performed after a harsh touch stimulus at the tail and worm locomotion was observed and measured 20 or 30 seconds after the stimulus. Body and head bends, reversals, duration of stillness periods and movement duration until the first stop were measured. In both cases, experiment was performed at least twice.

Pharynx pumping assay

L4 *fer*-15*(b26) II* and *myt-1(pan8) I; fer-15(b26) II* worms were individually transferred on NGM plates seeded with OP50 bacteria and kept at 25 °C until the experiment (see graphs/figure legends for details). Pharyngeal pumping rate was assessed as reported (50). Briefly, at least four 10-second videos separated by intervals of 20 seconds were recorded for each worm using a digital camera (Leica IC80HD, 29 frames/second) at 31,5x magnification and replayed at one third of the original speed to count the number of worm grinder movements. Finally, pumps per minute (ppm) were calculated for each animal.

Autophagosome/lysosome analysis

myt-1(pan8) I animals were crossed with DA2123 (*adIs2122 [lgg-1p::GFP::lgg-1 + rol-6(su1006)]*) (51) or MAH215 (*sqIs11* [*lgg-1p::mCherry::GFP::lgg-1 + rol-6(su1006)*]) worm strains and autophagosomal pool size was evaluated in adult worms compared to control animals of same age (3-day-old worms or L4/young adult stage, respectively), both in basal fed condition or after 24 h starvation in agitation at room temperature in M9 buffer. Worms were anesthetized with 10 mM NaN_3, mounted live on a 2% agarose pad and Z- stack images of the pharynx posterior bulb and of body wall muscles were acquired using a Leica TCS SP5 scanning confocal microscope with 0.6 µm slice intervals at 63x, as previously described(52). Images were manually analysed counting GFP::LGG-1 positive puncta in the posterior bulb of the pharynx, while mCherry::LGG-1 puncta (autolysosomes) were quantified in the posterior bulb of the pharynx and in the body wall muscle. At least two independent experiments were performed.

Statistics summary

All data are expressed as mean values ± SEM. The specific test analysis of each panel is reported in the single Excel (XLS) of Data availability. For survival curves Log-rank (Mantel-Cox) test was used. SPSS and Graphpad Prism 8 were used to calculate mean, median and chi square values for survival curves between groups. All data of this study was firstly tested for normality to perform a parametric or non-parametric statistical test. Parametric tests were used only where a normal distribution is assumed. Comparisons between 2 groups were done by 2-tailed Student's t tests. To determine if there is a significant difference between more than 2 groups, a

1-way ANOVA was used. Kruskal-Wallis test was used when the measurement variable does not meet the normality assumption of a one-way ANOVA. GraphPad Prism 8 (Statistical software) was used for all statistical analyses. A p-value <0.05 was considered statistically significant. In all figures *p<0.05, **p<0.01, ***p<0.001, ****p<0.0001.

Study approval

For human data, written informed consent was obtained from all patients, and the study was approved by the responsible Ethical Committee of Istituto Ortopedico Rizzoli (protocol no. 10823, issued on 26 April 2010) (Bologna–Italy).

Animal studies were approved by the Italian Ministero della Salute, Ufficio VI (authorization numbers 1060/2015) and by Ethics Committee of the University of Padova.

Data availability

Supporting data values presented in this article and the specific test analysis of each panel are openly available into a single Excel (XLS) file with separate tabs for each applicable figure panel.

The mass spectrometry proteomics data have been deposited to the ProteomeXchange Consortium via the PRIDE(53) partner repository with the dataset identifier PXD022180.

AUTHOR CONTRIBUTION

The number of experiments performed by each researcher was the method used for assigning the order of the two co- first authors. A.F-R designed and performed both mammal and *C. elegans* experiments, analysed data, interpret results, designed the figures and wrote the manuscript. V.M performed *C. elegans* experiments, generated the C2C12 MYTHO KO cell line, analysed data, interpret results and helped writing the manuscript. G.M, R.S and H.B.J.J. designed and performed some experiments. J.V.L performed statistical Cox proportional analysis. L.P, S.M generated the worm KO model by CRISPR-CAS9 technology. J.W. and P.G generated the endogenous MYTHO-HA cells. V.B and P.G generated the overexpressed HA-MYTHO stable cell line and performed the mass spectrometry analysis. A.A provided us muscle lysates of aged mice. I.D, V.R and F.C helped in interpreting results. MyoAtlas figure panels were elaborated

from D.P.M published snRNAseq project. Human biopsies were obtained from M.C, S.S and C.F. E.T, L.S and S.A.T helped in writing the manuscript, interpret the results and editing the manuscript. M.S conceived the project, planned experiments, interpreted the results and wrote the manuscript.

ACKNOWLEDGMENTS

This work was supported by AFM-Telethon (22982), AIRC (23257), PRIN 2022 (2022LZARA3), ASI (MARS-PRE), CARIPARO, Next Generation EU in the context of the National Recovery and Resilience Plan, Investment PE8 – Project Age-It: "Ageing Well in an Ageing Society" to MS; was supported by the Italian Ministry of Health (GR-2016-02362779), PRIN (2017BJJ5EE_003), CARIPARO (20/19 FCR) to E.T.; H.B.J.J. and S.T were supported by the Francis Crick Institute, which receives its core funding from Cancer Research UK (CC2134) the UK Medical Research Council (CC2134) and the Welcome Trust (CC2134); F.C. was supported by the Wellcome Trust/Royal Society (Sir Henry Dale Fellowship 102532/Z/12/Z and 102531/Z/13/A). Funded by the DFG, German Research Foundation – EXC 2030 -390661388. We are grateful to Marius Lemberg and Michael Knop for the support in the endogenous tagging. We thank the mass spectrometry and microscopy facilities at TIGEM Institute for the technical support. Strains were provided by the *Caenorhabditis* Genetics Center, which is funded by NIH Office of Research Infrastructure Programs (P40 OD010440). We also thank WormBase.

REFERENCES

1. Leidal AM, Levine B, and Debnath J. Autophagy and the cell biology of age-related disease. *Nat Cell Biol.* 2018;20(12):1338-48.
2. Kenyon C, Chang J, Gensch E, Rudner A, and Tabtiang R. A C. elegans mutant that lives twice as long as wild type. *Nature.* 1993;366(6454):461-4.
3. Johnson TE. Increased life-span of age-1 mutants in Caenorhabditis elegans and lower Gompertz rate of aging. *Science.* 1990;249(4971):908-12.
4. Ogg S, Paradis S, Gottlieb S, Patterson GI, Lee L, Tissenbaum HA, et al. The Fork head transcription factor DAF-16 transduces insulin-like metabolic and longevity signals in C. elegans. *Nature.* 1997;389(6654):994-9.
5. Lin K, Dorman JB, Rodan A, and Kenyon C. daf-16: An HNF-3/forkhead family member that can function to double the life-span of Caenorhabditis elegans. *Science.* 1997;278(5341):1319-22.
6. Webb AE, and Brunet A. FOXO transcription factors: key regulators of cellular quality control. *Trends in biochemical sciences.* 2014;39(4):159-69.
7. Martins R, Lithgow GJ, and Link W. Long live FOXO: unraveling the role of FOXO proteins in aging and longevity. *Aging Cell.* 2016;15(2):196-207.
8. Friedman DB, and Johnson TE. A mutation in the age-1 gene in Caenorhabditis elegans lengthens life and reduces hermaphrodite fertility. *Genetics.* 1988;118(1):75-86.
9. Lopez-Otin C, Blasco MA, Partridge L, Serrano M, and Kroemer G. The hallmarks of aging. *Cell.* 2013;153(6):1194-217.
10. Carnio S, LoVerso F, Baraibar MA, Longa E, Khan MM, Maffei M, et al. Autophagy impairment in muscle induces neuromuscular junction degeneration and precocious aging. *Cell Rep.* 2014;8(5):1509-21.
11. Fernandez AF, Sebti S, Wei Y, Zou Z, Shi M, McMillan KL, et al. Disruption of the beclin 1-BCL2 autophagy regulatory complex promotes longevity in mice. *Nature.* 2018;558(7708):136-40.
12. Madeo F, Zimmermann A, Maiuri MC, and Kroemer G. Essential role for autophagy in life span extension. *J Clin Invest.* 2015;125(1):85-93.
13. Melendez A, Talloczy Z, Seaman M, Eskelinen EL, Hall DH, and Levine B. Autophagy genes are essential for dauer development and life-span extension in C. elegans. *Science.* 2003;301(5638):1387-91.
14. Mizushima N, and Levine B. Autophagy in Human Diseases. *N Engl J Med.* 2020;383(16):1564-76.
15. Mizushima N. The ATG conjugation systems in autophagy. *Curr Opin Cell Biol.* 2020;63:1-10.
16. Sawa-Makarska J, Baumann V, Coudevylle N, von Bulow S, Nogellova V, Abert C, et al. Reconstitution of autophagosome nucleation defines Atg9 vesicles as seeds for membrane formation. *Science.* 2020;369(6508).
17. Sebastian D, and Zorzano A. Self-Eating for Muscle Fitness: Autophagy in the Control of Energy Metabolism. *Dev Cell.* 2020;54(2):268-81.
18. Stoeger T, Gerlach M, Morimoto RI, and Nunes Amaral LA. Large-scale investigation of the reasons why potentially important genes are ignored. *PLoS biology.* 2018;16(9):e2006643.
19. Milan G, Romanello V, Pescatore F, Armani A, Paik JH, Frasson L, et al. Regulation of autophagy and the ubiquitin-proteasome system by the FoxO transcriptional network during muscle atrophy. *Nat Commun.* 2015;6:6670.
20. Petrany MJ, Swoboda CO, Sun C, Chetal K, Chen X, Weirauch MT, et al. Single-nucleus RNA-seq identifies transcriptional heterogeneity in multinucleated skeletal myofibers. *Nat Commun.* 2020;11(1):6374.

21. Huang C, Xiong C, and Kornfeld K. Measurements of age-related changes of physiological processes that predict lifespan of Caenorhabditis elegans. *Proc Natl Acad Sci U S A.* 2004;101(21):8084-9.
22. Mizushima N, Yamamoto A, Matsui M, Yoshimori T, and Ohsumi Y. In vivo analysis of autophagy in response to nutrient starvation using transgenic mice expressing a fluorescent autophagosome marker. *Mol Biol Cell.* 2004;15(3):1101-11.
23. Fueller J, Herbst K, Meurer M, Gubicza K, Kurtulmus B, Knopf JD, et al. CRISPR-Cas12a-assisted PCR tagging of mammalian genes. *J Cell Biol.* 2020;219(6).
24. Kojima W, Yamano K, Kosako H, Imai K, Kikuchi R, Tanaka K, et al. Mammalian BCAS3 and C16orf70 associate with the phagophore assembly site in response to selective and non-selective autophagy. *Autophagy.* 2021;17(8):2011-36.
25. McKay JP, Raizen DM, Gottschalk A, Schafer WR, and Avery L. eat-2 and eat-18 are required for nicotinic neurotransmission in the Caenorhabditis elegans pharynx. *Genetics.* 2004;166(1):161-9.
26. Chi C, Ronai D, Than MT, Walker CJ, Sewell AK, and Han M. Nucleotide levels regulate germline proliferation through modulating GLP-1/Notch signaling in C. elegans. *Genes Dev.* 2016;30(3):307-20.
27. Berry LW, Westlund B, and Schedl T. Germ-line tumor formation caused by activation of glp-1, a Caenorhabditis elegans member of the Notch family of receptors. *Development.* 1997;124(4):925-36.
28. Arantes-Oliveira N, Apfeld J, Dillin A, and Kenyon C. Regulation of life-span by germ-line stem cells in Caenorhabditis elegans. *Science.* 2002;295(5554):502-5.
29. Hansen M, Chandra A, Mitic LL, Onken B, Driscoll M, and Kenyon C. A role for autophagy in the extension of lifespan by dietary restriction in C. elegans. *PLoS Genet.* 2008;4(2):e24.
30. Bakula D, Muller AJ, Zuleger T, Takacs Z, Franz-Wachtel M, Thost AK, et al. WIPI3 and WIPI4 beta-propellers are scaffolds for LKB1-AMPK-TSC signalling circuits in the control of autophagy. *Nat Commun.* 2017;8:15637.
31. Huttlin EL, Bruckner RJ, Paulo JA, Cannon JR, Ting L, Baltier K, et al. Architecture of the human interactome defines protein communities and disease networks. *Nature.* 2017;545(7655):505-9.
32. Dooley HC, Razi M, Polson HE, Girardin SE, Wilson MI, and Tooze SA. WIPI2 links LC3 conjugation with PI3P, autophagosome formation, and pathogen clearance by recruiting Atg12-5-16L1. *Mol Cell.* 2014;55(2):238-52.
33. Fracchiolla D, Chang C, Hurley JH, and Martens S. A PI3K-WIPI2 positive feedback loop allosterically activates LC3 lipidation in autophagy. *J Cell Biol.* 2020;219(7).
34. Harada K, Kotani T, Kirisako H, Sakoh-Nakatogawa M, Oikawa Y, Kimura Y, et al. Two distinct mechanisms target the autophagy-related E3 complex to the pre-autophagosomal structure. *Elife.* 2019;8.
35. Nishimura T, Kaizuka T, Cadwell K, Sahani MH, Saitoh T, Akira S, et al. FIP200 regulates targeting of Atg16L1 to the isolation membrane. *EMBO Rep.* 2013;14(3):284-91.
36. Lystad AH, Carlsson SR, de la Ballina LR, Kauffman KJ, Nag S, Yoshimori T, et al. Distinct functions of ATG16L1 isoforms in membrane binding and LC3B lipidation in autophagy-related processes. *Nat Cell Biol.* 2019;21(3):372-83.
37. Dudley LJ, Cabodevilla AG, Makar AN, Sztacho M, Michelberger T, Marsh JA, et al. Intrinsic lipid binding activity of ATG16L1 supports efficient membrane anchoring and autophagy. *EMBO J.* 2019;38(9).
38. Jelani M, Dooley HC, Gubas A, Mohamoud HSA, Khan MTM, Ali Z, et al. A mutation in the major autophagy gene, WIPI2, associated with global developmental abnormalities. *Brain.* 2019;142(5):1242-54.
39. Yoshihara K, Wang Q, Torres-Garcia W, Zheng S, Vegesna R, Kim H, et al. The landscape and therapeutic relevance of cancer-associated transcript fusions. *Oncogene.* 2015;34(37):4845-54.

40. Leduc-Gaudet JP, Franco-Romero A, Cefis M, Moamer A, Broering FE, Milan G, et al. MYTHO is a novel regulator of skeletal muscle autophagy and integrity. *Nat Commun.* 2023;14(1):1199.
41. Paix A, Folkmann A, Rasoloson D, and Seydoux G. High Efficiency, Homology-Directed Genome Editing in Caenorhabditis elegans Using CRISPR-Cas9 Ribonucleoprotein Complexes. *Genetics.* 2015;201(1):47-54.
42. Hobert O. PCR fusion-based approach to create reporter gene constructs for expression analysis in transgenic C. elegans. *BioTechniques.* 2002;32(4):728-30.
43. Wang H, Liu J, Gharib S, Chai CM, Schwarz EM, Pokala N, et al. cGAL, a temperature-robust GAL4-UAS system for Caenorhabditis elegans. *Nat Methods.* 2017;14(2):145-8.
44. Jacomin AC, Samavedam S, Promponas V, and Nezis IP. iLIR database: A web resource for LIR motif-containing proteins in eukaryotes. *Autophagy.* 2016;12(10):1945-53.
45. Puntervoll P, Linding R, Gemund C, Chabanis-Davidson S, Mattingsdal M, Cameron S, et al. ELM server: A new resource for investigating short functional sites in modular eukaryotic proteins. *Nucleic Acids Res.* 2003;31(13):3625-30.
46. Dillin A, Crawford DK, and Kenyon C. Timing requirements for insulin/IGF-1 signaling in C. elegans. *Science.* 2002;298(5594):830-4.
47. Hsin H, and Kenyon C. Signals from the reproductive system regulate the lifespan of C. elegans. *Nature.* 1999;399(6734):362-6.
48. Sawin ER, Ranganathan R, and Horvitz HR. C. elegans locomotory rate is modulated by the environment through a dopaminergic pathway and by experience through a serotonergic pathway. *Neuron.* 2000;26(3):619-31.
49. Chiba CM, and Rankin CH. A developmental analysis of spontaneous and reflexive reversals in the nematode Caenorhabditis elegans. *Journal of neurobiology.* 1990;21(4):543-54.
50. Raizen D, Song BM, Trojanowski N, and You YJ. Methods for measuring pharyngeal behaviors. *WormBook.* 2012:1-13.
51. Kang C, You YJ, and Avery L. Dual roles of autophagy in the survival of Caenorhabditis elegans during starvation. *Genes Dev.* 2007;21(17):2161-71.
52. Chang JT, Kumsta C, Hellman AB, Adams LM, and Hansen M. Spatiotemporal regulation of autophagy during Caenorhabditis elegans aging. *Elife.* 2017;6.
53. Perez-Riverol Y, Csordas A, Bai J, Bernal-Llinares M, Hewapathirana S, Kundu DJ, et al. The PRIDE database and related tools and resources in 2019: improving support for quantification data. *Nucleic Acids Res.* 2019;47(D1):D442-D50.

FIGURE LEGENDS

Figure 1 C16orf70 encodes for a protein, named MYTHO that is expressed in different tissues and upregulated in ageing. (**A**) PBI-eGFP/3xFlag-MYTHO vector or PBI-eGFP/3xFlag-empty vector was transfected into HEK293A cells. 3xFlag-MYTHO expression is observed using anti-Flag antibody. The blot shown in the image represents the results of four independent transfections. **(B)** Quantitative RT-PCR of *Mytho* in different organs and muscles from 5 months old male mice. mRNA expression was calculated with Delta Ct method and expressed as fold increase from the tissue where *Mytho* is less expressed (small intestine). SOL (Soleus muscle), GNM (Gastrocnemius muscle), EDL (Extensor digitorum longus muscle), TA (Tibialis anterior muscle), QUAD (Quadriceps muscle), WAT (White adipose tissue), BAT (Brown adipose tissue). n=3 for all tissues, n=2 only for WAT and lung. (**C**) Quantitative real time PCR of *Mytho* from mice of different age (3-4 months (n=5), 7 months (n=4), 10 months (n=6) and >2 years old mice (n=4)). Normalization was performed on *Gapdh* and expressed as fold increase (1-way ANOVA) (**D**) Quantitative real time PCR of *MYTHO* in muscle biopsies from patients of different ages: 24-38 years old (n=8), 45-64 years old (n=7), 67-75 years old (n=7), 84-95 years old patients with hip fracture knee problems (n=8). All data are normalized to *GAPDH* and expressed as fold increase from 24-38 years old control group (1-way ANOVA). **(E)** Immunoblot of homogenates from GNM muscle from 5 months old mice (n=4) and >24 months old (n=6) mice. C16orf70 antibody was used to detect MYTHO endogenous protein. Normalization was performed on GAPDH and expressed as fold increase (student's t-test 2-tailed). All Bars indicate S.E.M. *p<0.05 **p<0.01

Figure 2 *Mytho* expression increases in muscle during ageing. snRNAseq data re-elaborated from MYOATLAS *(https://research.cchmc.org/myoatlas/)*. **(A**) UMAP showing snRNAseq expression of *Mytho* in different cell population from 5-month old SOL muscle. (**B**) Violin plots with the quantification of *Mytho* expression in the different cell types. (**C**) UMAP of the different population of snRNAseq showing *Mytho* expression at 5 months and 30 months. (**D**) Violin plots showing nucleus transcriptomic profiles of *Mytho* gene in myonuclei type 2X, myonuclei NMJ and Schwann cells of animals at different ages. (p10: postnatal day 10, p21: postnatal day 21, 5m: 5 months, 24m: 24 months, 30m: 30 months, TA: Tibialis Anterior)

Figure 3 *Mytho* depletion induces cellular senescence (**A**) The graph shows the logarithm (log) of total number of cells measured at 2 days, 4 days and 8 days after seeded. Cellular confluence was reached at 4 and 8 days in control and *Mytho* deficient cells, respectively(N=3) (Student's t-test 2-tailed). (**B**) Quantitative real time PCR of *p21* from WT and *Mytho* KO C2C12 cells normalized on *Gapdh* and expressed as fold increase (N=3) (Student's t-test 2-tailed). (**C**) Electron-microscopy representative images of the cytoplasm of WT(up) and *Mytho* KO(down) C2C12 cells. Abnormal swollen mitochondria are often found in KO cells. Scale bar =1µm. (**D**) Mt-roGFP fluorescence was measured in single cells (n=30/condition) in N=2. Arrow indicates the addition of H_2O_2. (**E**) % senescence in cells measured by FACS after WT and *Mytho* KO C2C12 cells were incubated with Cell Senescence Prove (N=3) (Multiple unpaired t-test). All Bars indicate S.E.M. $^{**}p<0.01$ $^{****}p<0.0001$

Figure 4. *Mytho* depletion reduces *C. elegans* lifespan and health span. (**A**) Survival curves of *fer-15(b26) II* and *myt-1(pan8) I; fer-15(b26) II* worms (n=521, N=5). **(B)** Survival curves of *fer-15(b26) II* worms fed with either bacteria transformed with pL4440 empty vector (n=252) or with pL4440 containing *myt-1* coding sequence (*myt-1(RNAi)*, n=253) following a maternal RNAi protocol (see Materials and methods) (N=3). (**C**) Total number of body bends, reversals and duration of stillness periods calculated for 5-day-old *fer-15(b26) II* (n=15) and *myt-1(pan8) I; fer-15(b26) II* (n=17) animals in spontaneous locomotion (N=3). Pumping rate (pumps/minute) was assessed at day 1 (YOUNG, n=20; n=20) and day 5 (OLD, n=19; n=18) in *fer-15(b26) II* and *myt-1(pan8) I; fer-15(b26) II* animals (N=2). **(D)** Spontaneous locomotion analysis of body and head bends, reversals and duration of stillness periods in 11-day-old *fer-15(b26) II* animals fed with *myt-1(RNAi)*) (n=17) or control bacteria (n=21) (N=2). Log-rank (Mantel-Cox) test was used to compare longevity curves in graphs A and B (See figure S6A for lifespan experiments details and statistics). Bars of figures C and D indicate S.E.M $^{*}p<0.05$. $^{**}p<0.01$, $^{****}p<0.0001$ (Student's *t*-test 2-tailed). N=number of independent experiments. n=total number of individuals.

Figure 5 Depletion of *Mytho* reduces autophagic flux in vitro and in vivo. (**A**) Left panel: representative images of HEK293 cells transfected with MYTHO-GFP. Right panel:

representative image of endogenous MYTHO. Scale bar=10µm. **(B)** Left panel: FDB muscles transfected with MYTHO-GFP. Right panel: endogenous Mytho in FDB fibers. Scale bar = 10µm. (**C**) Endogenously HA-tagged Mytho co-immunoprecipitates with LC3B. The asterisk (*) indicates an aspecific band. (**D**) LC3 lipidation was analysed by immunoblot in WT and *Mytho* KO C2C12 cells treated or not with chloroquine. LC3-II band was normalized to GAPDH (n=8) (Student's t-test 2-tailed) (**E**) On the left representative fluorescent images of WT and *Mytho* KO C2C12 cells transfected with Cherry-LC3B and treated with chloroquine or vehicle. Scale bar=10µm. On the right, the quantification of LC3 puncta/area of the cell in each condition is shown (n>15 cells/condition) (1-way ANOVA). **(F)** Above, representative fluorescent images of GFP::LGG-1 puncta in the posterior bulb of the pharynx of N2(WT) and *myt-1(pan8) I* worms. Scale bar=25µm. Below, autophagosomal pool quantification in WT (n=26), *myt-1(pan8*) *I* (n=20) worms (N=3) (Student's *t*-test 2-tailed) (**G-H**) Above, representative fluorescent images of mCherry::LGG-1 puncta in the posterior bulb of the pharynx **(G)** and in body wall muscle **(H)** of N2 (WT) and *myt-1(pan8) I* worms. Scale bar=25µm (G) and 50µm (H). Below, relative quantification of mCherry::LGG-1 puncta in basal condition and after 24 h starvation in M9 buffer. WT FED (n=14), *myt-1(pan8*) *I* FED (n=22), WT STV 24 h (n=17), *myt-1(pan8) I* STV 24 h (n=27); N=2. (Student's *t*-test 2-tailed) **(I)** Above, representative fluorescent images of single fibers from FDB muscle transfected with YFP-LC3/3xFlagMYTHO- or YFP-LC3/Flag-empty in basal condition. Scale bar=20µm. Below, quantification of LC3 puncta in >12 fibers (Student's t-test 2-tailed). All Bars indicate S.E.M $*p<0.05$ $**p<0.01$ $***p<0.001$ $****p<0.0001$ N=number of independent experiments. n=number of cells/samples

Figure 6 MYTHO interacts with autophagic proteins. (A) Mass spectrometry analysis of immunoprecipitated endogenous-HA tagged MYTHO. Significant autophagic-related proteins are shown in the graph. **(B)** Quantification of WIPI2 puncta in FED and starved (2 hrs) conditions in WT and *Mytho* KO C2C12 cells in N=3. FED WT (n=141); FED *Mytho* KO (n=144), EBSS 2 h WT (n=139); EBSS 2 h *Mytho* KO (n=172). Bars indicate S.E.M. ****p<0.0001. (1-way ANOVA). **(C)** HEK293 cells transfected with WIPI2-GFP or GFP were immunoprecipitated with GFP-trap. The quantification of N=3 (normalized by input) is shown in fig S9E. (**D**) HEK293 cells transfected with MYTHO-GFP or GFP were immunoprecipitated. Endogenous WIPI2, ATG7 and BCAS3 were blotted. In the blot on the left lanes were run on the

same gel but were non-contiguous. The quantification of N=3 (normalized by input) is represented in fig S9F. N=number of independent experiments. n=number of cells/samples

Figure 7 MYTHO is required for WIPI2 and BCAS3 location on autophagosomes (A) Representative scheme showing predicted LC3 interaction motifs and WD40 domains: Y91A/V94A(M1); F131A/L134A(M2); Y288A/L291A(M3); W351A/I354A(M4); 208delTGPSGLRLRL(M5) or Y288A/L291A + 208delTGPSGLRLRL(M3/M5). (**B-C**) HEK293 cells transfected with GFP, MYTHO-GFP or MYTHO-GFP mutants were lysed immunoprecipitated with GFP-TRAP, and blotted with indicated markers. All samples were run on the same gel. Quantification of LC3, WIPI2 and BCAS3 enrichment (normalized by input) is shown in Fig S10B-D (N=3). **(D)** HEK293 cells were transfected with the following vectors: empty (GFP), GFP-WIPI2 or WIPI2 mutants (GFP-RERE (R108E/R128E), GFP-FTTG or double mutant). Immunoprecipitation was performed as in B and C, and endogenous BCAS3 or MYTHO were blotted. **(E)** Above, representative fluorescent images of endogenous WIPI2 protein in *Mytho* KO cells transfected with GFP or MYTHO-GFP vector. Scale bar = 20µm. Below, quantification of WIPI2 puncta/cell in FED and 2h starvation(N=3) using ImageJ software. FED WT + GFP (n=34); FED *Mytho* KO + GFP (n=69), FED *Mytho* KO + MYTHO-GFP (n=49); HBSS 2h WT + GFP (n=12); HBSS 2h *Mytho* KO + GFP (n=53), HBSS 2h *Mytho* KO + MYTHO-GFP (n=33) (ANOVA Kruskal-Wallis test). **(F-G)** WT and *Mytho* KO C2C12 cells were transfected with empty (GFP), MYTHO-GFP (WT), M1-GFP, M3-GFP, M5-GFP or M3/M5-GFP vectors. The quantification of endogenous LC3 (F) or WIPI2 (G) puncta in fed condition was performed using the ImageJ software (N=3). For LC3 puncta: WT+GFP (n=91); *Mytho* KO + GFP (n=101), *Mytho* KO+WT (n=84); *Mytho* KO+M1 (n=41); *Mytho* KO+M3 (n=48), *Mytho* KO+M5 (n=40), *Mytho* KO + M3/M5 (n=53) (1-way ANOVA). For WIPI2 puncta: WT+GFP (n=107); *Mytho* KO + GFP (n=119), *Mytho* KO+WT (n=98); *Mytho* KO+M1 (n=65); *Mytho* KO+M3 (n=115), *Mytho* KO+M5 (n=50), *Mytho* KO+M3/M5 (n=56) (ANOVA Kruskal-Wallis test). All Bars indicate S.E.M. $**p<0.001$ $****p<0.0001$. N=number of independent experiments. n=number of samples.

Figure 8 *myt-1* controls longevity through the *eat-2* and *glp-1* signalling pathways. (A) Survival curves of *fer-15(b26) II* (n=140), *myt-1(pan8) I; fer-15(b26) II* (n=140), *fer-15(b26) II;*

daf-2(e1370) III (n=141) and *myt-1(pan8) I; fer-15(b26) II, daf-2(e1370) III* worms (n=179) (N=2). **(B)** Survival curves of *fer-15(b26) II* (n=216), *myt-1(pan8) I; fer-15(b26) II* (n=244), *fer-15(b26) II; eat-2(ad1116) II* (n=171) and *myt-1(pan8) I; fer-15(b26) II; eat-2(ad1116) II* (n=263) worms (N=2/3). **(C)** Survival curves of *fer-15(b26) II* (n=135), *myt-1(pan8) I; fer-15(b26) II* (n=162), *fer-15(b26) II; glp-1(e2141) III* (n=163), *myt-1(pan8) I; fer-15(b26) II; glp-1(e2141) III* (n=162) (N=2). Raw data of *fer-15(b26) II* and *myt-1(pan8) I; fer-15(b26) II* worms are the same in graph B and C (experiments were performed in parallel). Cox-proportional hazards analysis was performed for the interaction of terms genotypes *myt-1* and *daf-2* (0.00018), *eat-2* (0.00004), *glp-1* (0.0007). **(D-E)** Lifespan of young adult *fer-15(b26) II* and *myt-1(pan8) I; fer-15(b26) II* worms fed with empty pL4440 vector or pL4440 expressing the *atg-18* coding sequence (*atg-18(RNAi)*) (n=260-340 worms/condition) **(D)** or *bec-1* coding sequence (*bec-1(RNAi)*) (n=228-290 worms/condition) **(E)** following the adulthood RNAi protocol (see Materials and methods), (N=3). Cox-proportional hazards analysis was performed for the interaction of terms genotypes *myt-1* and *atg-18* RNAi (<0.0001), *bec-1* RNAi (0.01466). Raw data of *fer-15(b26) II* and *myt-1(pan8) I; fer-15(b26) II* worms are the same in graph D and E (experiments were performed in parallel). Log-rank test was used to compare longevity curves (See figure S6A for lifespan experiments details and statistics). **(F)** Body and head bends, reversals and duration of stillness periods were quantified for 30 seconds in 10-day-old *fer-15(b26) II* animals (WT) and *fer-15(b26) II; oxTi0882; syls321* (OE *myt-1*) worms fed with *atg-18(RNAi)* (n=38(WT)/n=51(OE *myt-1*)) or control bacteria (n=33(WT)/n=76(OE *myt-1*)) after a harsh touch stimulus at the tail(N=2). **p*<0.05, ***p<0.001, *****p*<0.0001. N=number of independent experiments. n=total worm number.

Figure 9: Scheme of MYTHO function in mammalian cells and C. elegans. Left panel shows the effects of MYTHO inhibition in mammalian cells. The ablation of Mytho gene caused autophagy impairment, mitochondrial dysfunction with increased ROS production, accumulation of β-galactosidase, upregulation of p21 and reduced cell proliferation. These features belong to the hallmarks of ageing supporting a MYTHO role in preventing cellular senescence. The right panel describes the consequences of myt-1 deletion in C.elegans . Consistently, autophagy flux, resistance to oxidative stress, life- and health-span were reduced in absence of myt-1. The myt-1

contribution to life-span were dissected by genetic interaction studies that identified a myt-1 involvement in glp-1 and eat-2 mediated longevity.

Figure 1

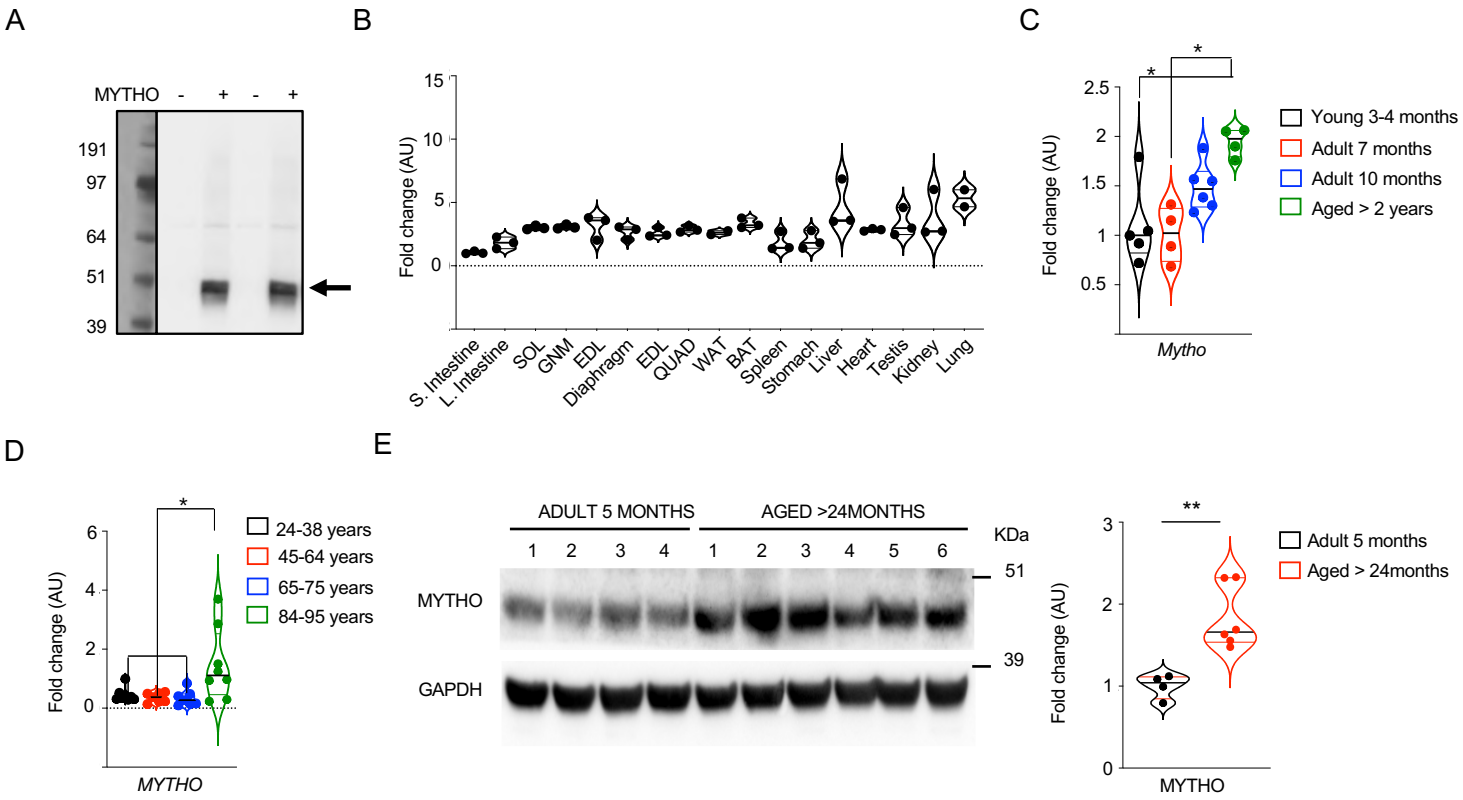
A
MYTHO - + - +
191
97
64
51
39
B
Fold change (AU)
15
10
5
0
S. Intestine
L. Intestine
SOL
GNM
EDL
Diaphragm
EDL
QUAD
WAT
BAT
Spleen
Stomach
Liver
Heart
Testis
Kidney
Lung
C
Fold change (AU)
2.5
2
1.5
1
0.5
*
*
Mytho
Young 3-4 months
Adult 7 months
Adult 10 months
Aged > 2 years
D
Fold change (AU)
6
4
2
0
*
MYTHO
24-38 years
45-64 years
65-75 years
84-95 years
E
ADULT 5 MONTHS
AGED >24MONTHS
1 2 3 4 1 2 3 4 5 6
KDa
MYTHO
GAPDH
51
39
Fold change (AU)
3
2
1
0
**
MYTHO
Adult 5 months
Aged > 24months

Figure 2

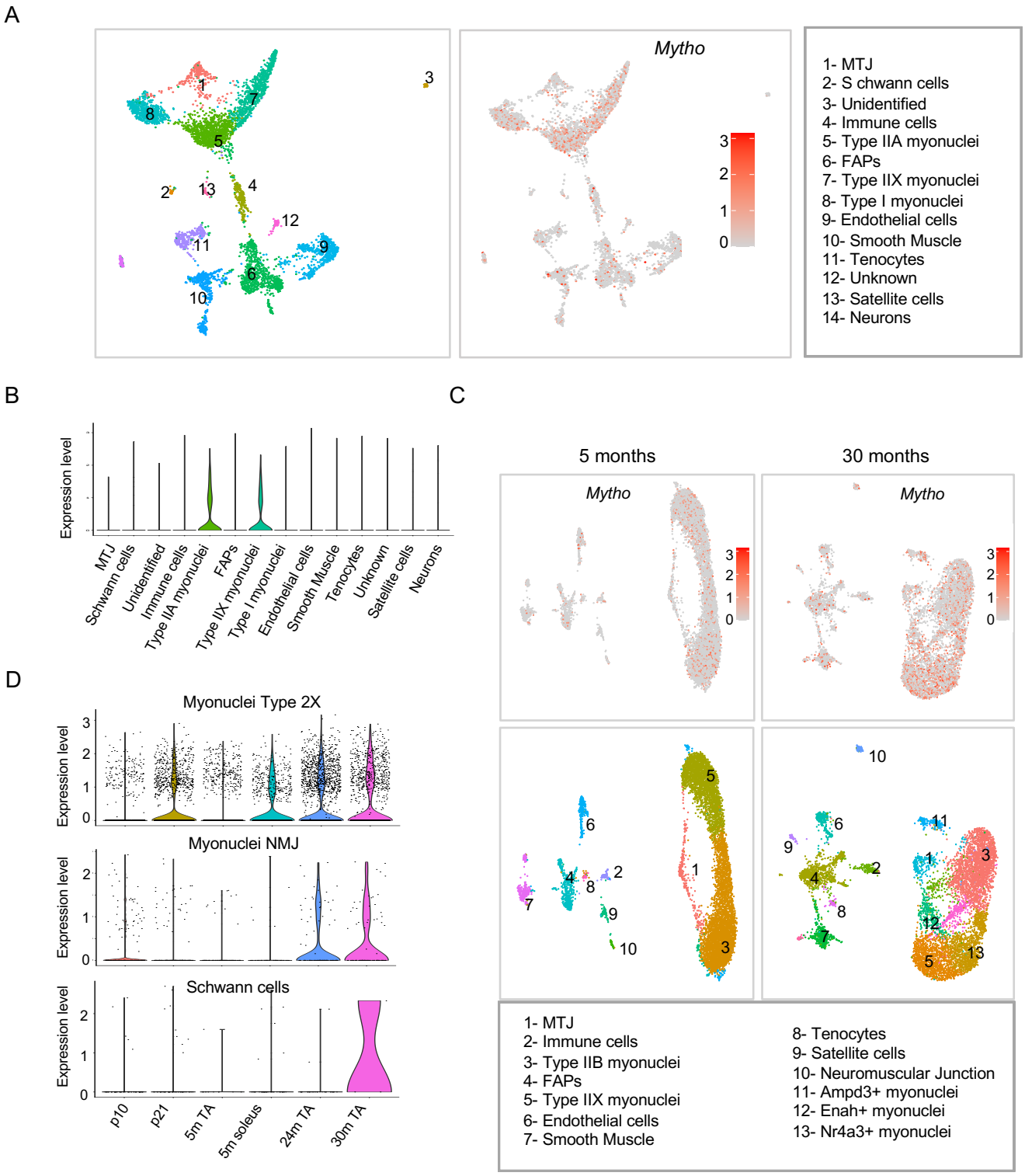
A
Mytho
1- MTJ
2- S chwann cells
3- Unidentified
4- Immune cells
5- Type IIA myonuclei
6- FAPs
7- Type IIX myonuclei
8- Type I myonuclei
9- Endothelial cells
10- Smooth Muscle
11- Tenocytes
12- Unknown
13- Satellite cells
14- Neurons
B
Expression level
MTJ
Schwann cells
Unidentified
Immune cells
Type IIA myonuclei
FAPs
Type IIX myonuclei
Type I myonuclei
Endothelial cells
Smooth Muscle
Tenocytes
Unknown
Satellite cells
Neurons
C
5 months
30 months
Mytho
D
Myonuclei Type 2X
Myonuclei NMJ
Schwann cells
p10
p21
5m TA
5m soleus
24m TA
30m TA
1- MTJ
2- Immune cells
3- Type IIB myonuclei
4- FAPs
5- Type IIX myonuclei
6- Endothelial cells
7- Smooth Muscle
8- Tenocytes
9- Satellite cells
10- Neuromuscular Junction
11- Ampd3+ myonuclei
12- Enah+ myonuclei
13- Nr4a3+ myonuclei

Figure 3

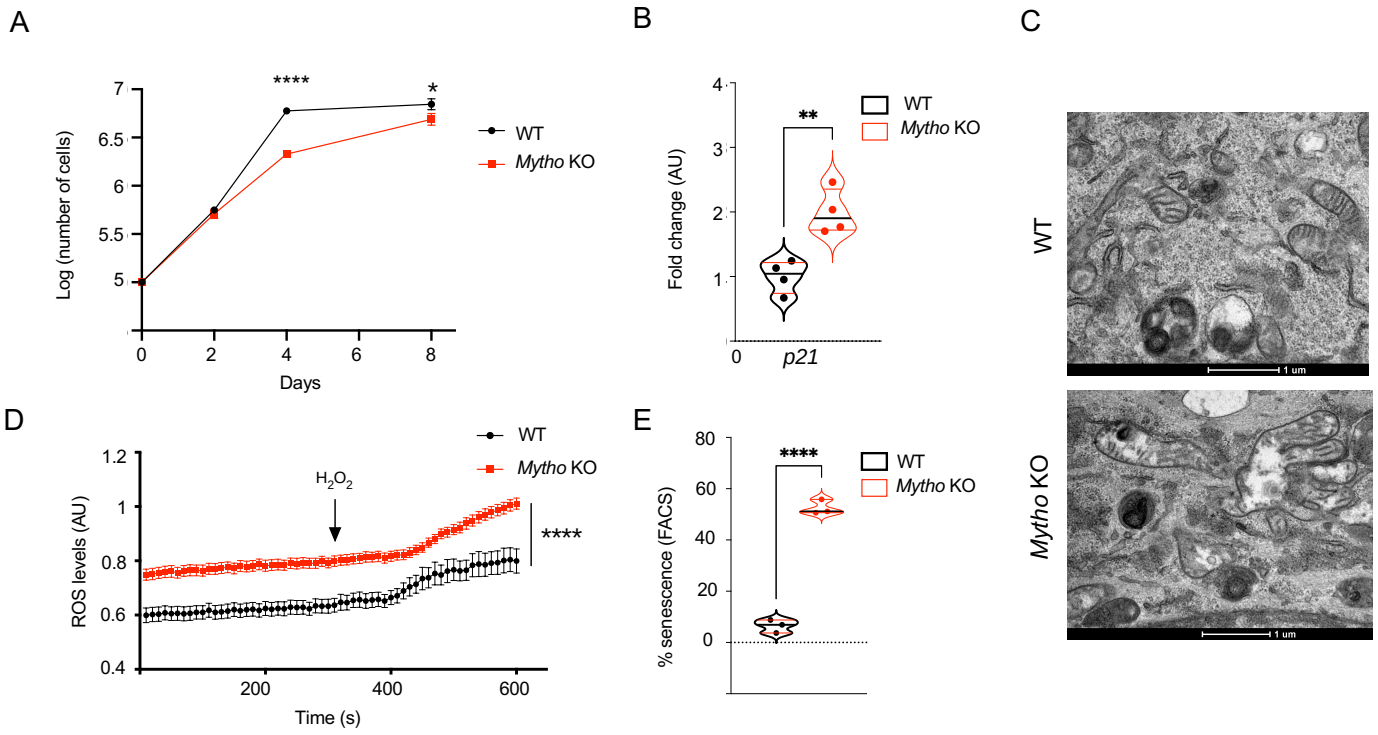
A
Log (number of cells)
Days
WT
Mytho KO
****
*
B
Fold change (AU)
p21
WT
Mytho KO
**
C
WT
Mytho KO
1 um
1 um
D
ROS levels (AU)
Time (s)
H2O2
WT
Mytho KO
****
E
% senescence (FACS)
WT
Mytho KO
****

Figure 4

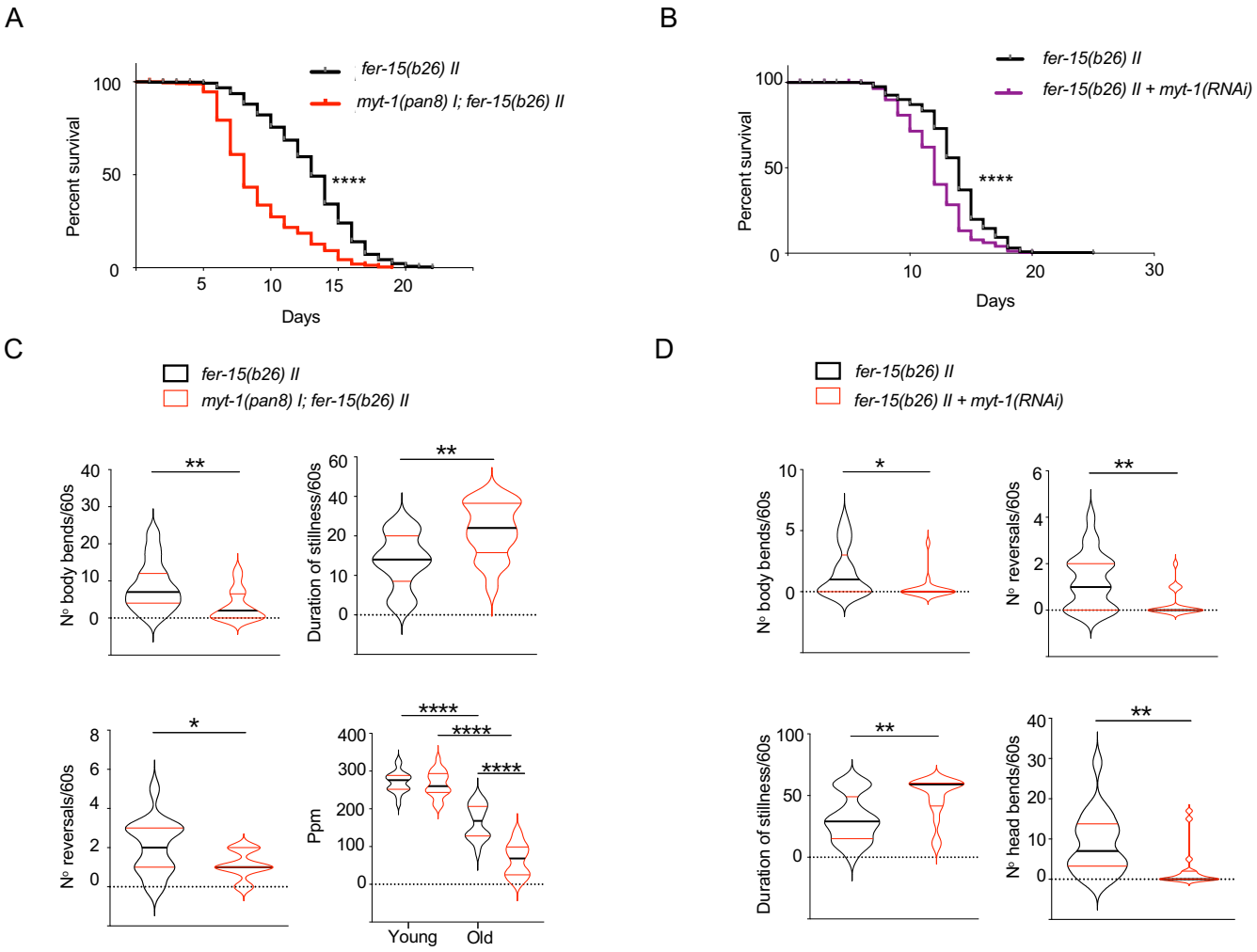
A
fer-15(b26) II
myt-1(pan8) I; fer-15(b26) II
Percent survival
Days
****
B
fer-15(b26) II
fer-15(b26) II + myt-1(RNAi)
Percent survival
Days
****
C
fer-15(b26) II
myt-1(pan8) I; fer-15(b26) II
Nº body bends/60s
Duration of stillness/60s
Nº reversals/60s
Ppm
Young
Old
D
fer-15(b26) II
fer-15(b26) II + myt-1(RNAi)
Nº body bends/60s
Nº reversals/60s
Duration of stillness/60s
Nº head bends/60s

Figure 5

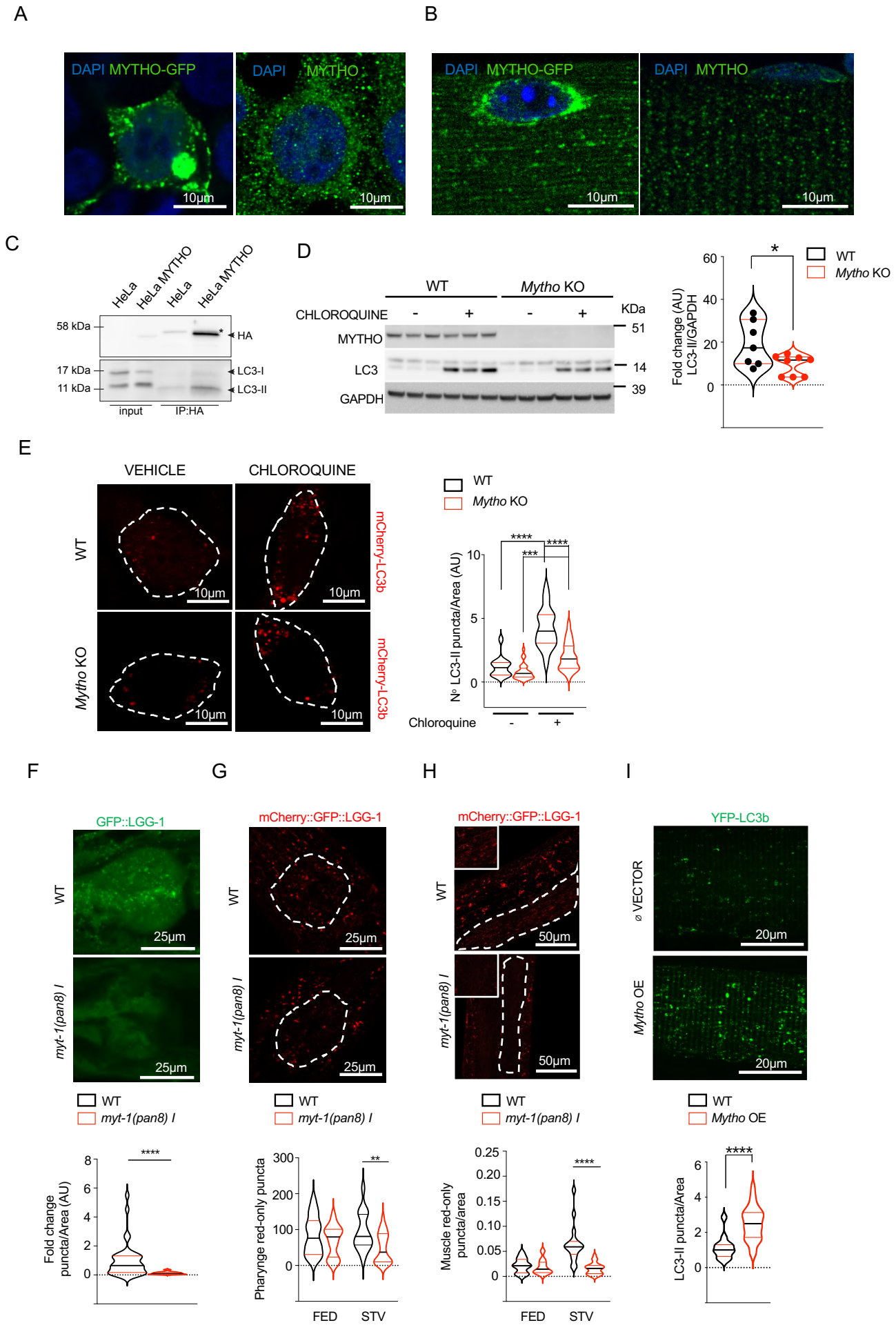
A
DAPI MYTHO-GFP
DAPI MYTHO
10µm
B
C
HeLa
HeLa MYTHO
58 kDa
HA
17 kDa
11 kDa
LC3-I
LC3-II
input
IP:HA
D
WT
Mytho KO
CHLOROQUINE
KDa
MYTHO
LC3
GAPDH
51
14
39
Fold change (AU) LC3-II/GAPDH
E
VEHICLE
CHLOROQUINE
mCherry-LC3b
Nº LC3-II puncta/Area (AU)
Chloroquine
F
GFP::LGG-1
myt-1(pan8) I
25µm
G
mCherry::GFP::LGG-1
H
50µm
I
YFP-LC3b
ø VECTOR
Mytho OE
20µm
Fold change puncta/Area (AU)
Pharynge red-only puncta
Muscle red-only puncta/area
LC3-II puncta/Area
FED
STV

Figure 6

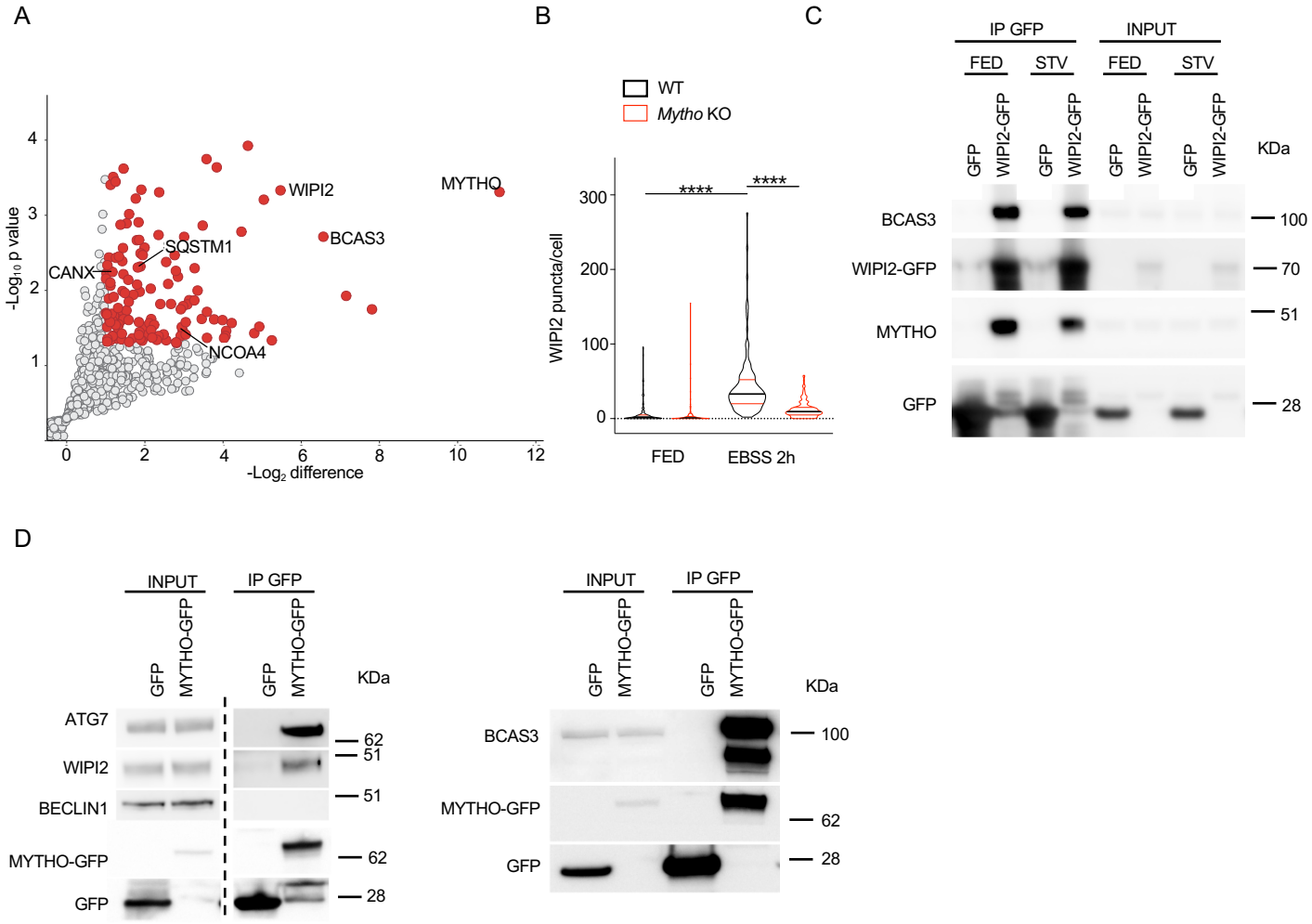
A
B
C
D
WIPI2
MYTHO
BCAS3
SQSTM1
CANX
NCOA4
-Log10 p value
-Log2 difference
WT
Mytho KO
WIPI2 puncta/cell
****
FED
EBSS 2h
IP GFP
INPUT
STV
KDa
BCAS3
WIPI2-GFP
MYTHO
GFP
ATG7
BECLIN1
MYTHO-GFP

Figure 7

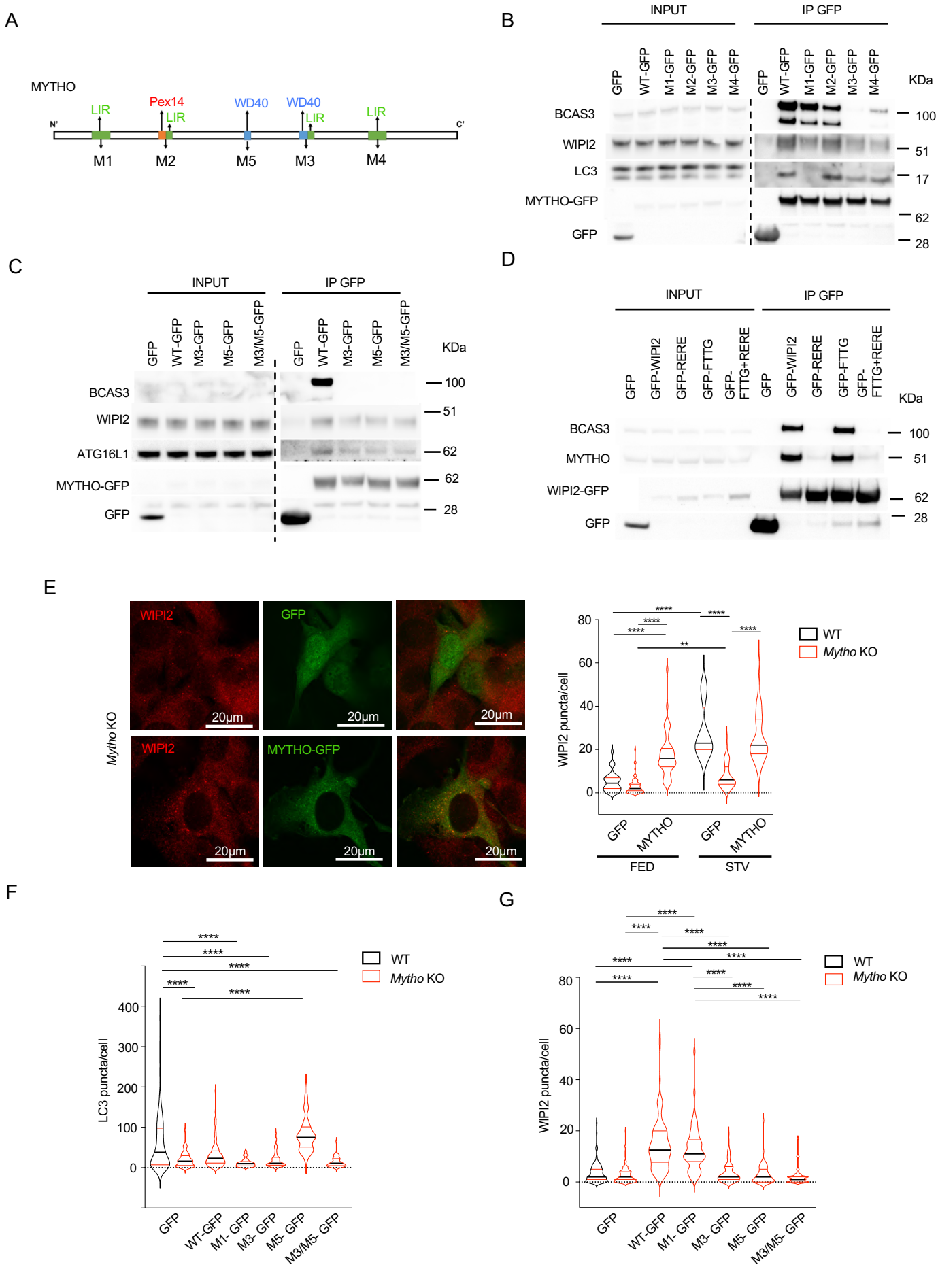
A
MYTHO
LIR
Pex14
LIR
WD40
WD40
LIR
LIR
N'
C'
M1
M2
M5
M3
M4
B
INPUT
IP GFP
GFP
WT-GFP
M1-GFP
M2-GFP
M3-GFP
M4-GFP
KDa
BCAS3
WIPI2
LC3
MYTHO-GFP
GFP
100
51
17
62
28
C
INPUT
IP GFP
GFP
WT-GFP
M3-GFP
M5-GFP
M3/M5-GFP
KDa
BCAS3
WIPI2
ATG16L1
MYTHO-GFP
GFP
100
51
62
62
28
D
INPUT
IP GFP
GFP
GFP-WIPI2
GFP-RERE
GFP-FTTG
GFP-FTTG+RERE
KDa
BCAS3
MYTHO
WIPI2-GFP
GFP
100
51
62
28
E
Mytho KO
WIPI2
GFP
MYTHO-GFP
20µm
WIPI2 puncta/cell
WT
Mytho KO
GFP
MYTHO
FED
STV
F
LC3 puncta/cell
WT
Mytho KO
GFP
WT-GFP
M1- GFP
M3- GFP
M5- GFP
M3/M5- GFP
G
WIPI2 puncta/cell
WT
Mytho KO
GFP
WT-GFP
M1- GFP
M3- GFP
M5- GFP
M3/M5- GFP

Figure 8

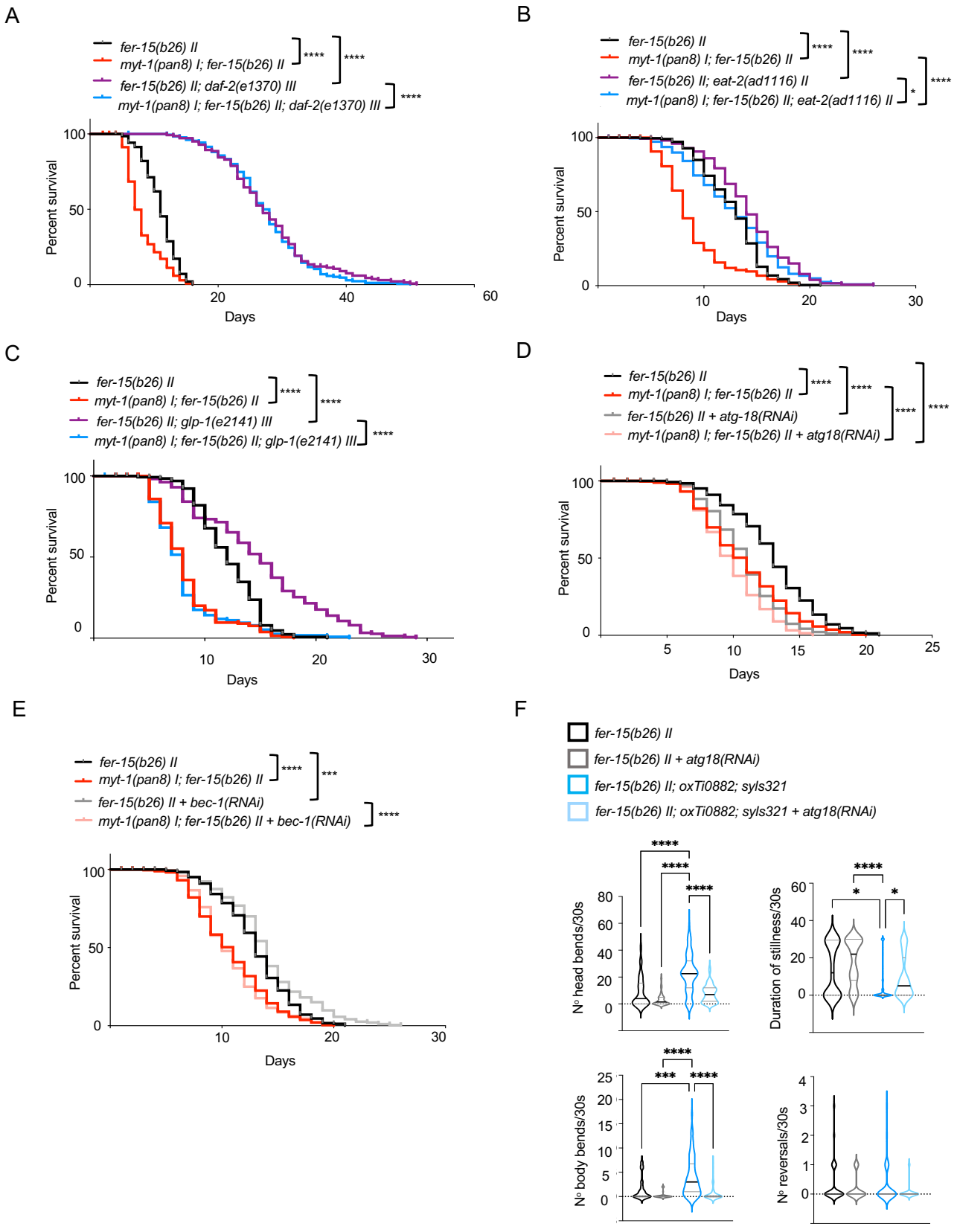
A
fer-15(b26) II
myt-1(pan8) I; fer-15(b26) II
fer-15(b26) II; daf-2(e1370) III
myt-1(pan8) I; fer-15(b26) II; daf-2(e1370) III
****
****
****
Percent survival
Days
B
fer-15(b26) II
myt-1(pan8) I; fer-15(b26) II
fer-15(b26) II; eat-2(ad1116) II
myt-1(pan8) I; fer-15(b26) II; eat-2(ad1116) II
****
****
*
****
Percent survival
Days
C
fer-15(b26) II
myt-1(pan8) I; fer-15(b26) II
fer-15(b26) II; glp-1(e2141) III
myt-1(pan8) I; fer-15(b26) II; glp-1(e2141) III
****
****
****
Percent survival
Days
D
fer-15(b26) II
myt-1(pan8) I; fer-15(b26) II
fer-15(b26) II + atg-18(RNAi)
myt-1(pan8) I; fer-15(b26) II + atg18(RNAi)
****
****
****
****
Percent survival
Days
E
fer-15(b26) II
myt-1(pan8) I; fer-15(b26) II
fer-15(b26) II + bec-1(RNAi)
myt-1(pan8) I; fer-15(b26) II + bec-1(RNAi)
****
***
****
Percent survival
Days
F
fer-15(b26) II
fer-15(b26) II + atg18(RNAi)
fer-15(b26) II; oxTi0882; syls321
fer-15(b26) II; oxTi0882; syls321 + atg18(RNAi)
Nº head bends/30s
Duration of stillness/30s
Nº body bends/30s
Nº reversals/30s

Figure 9

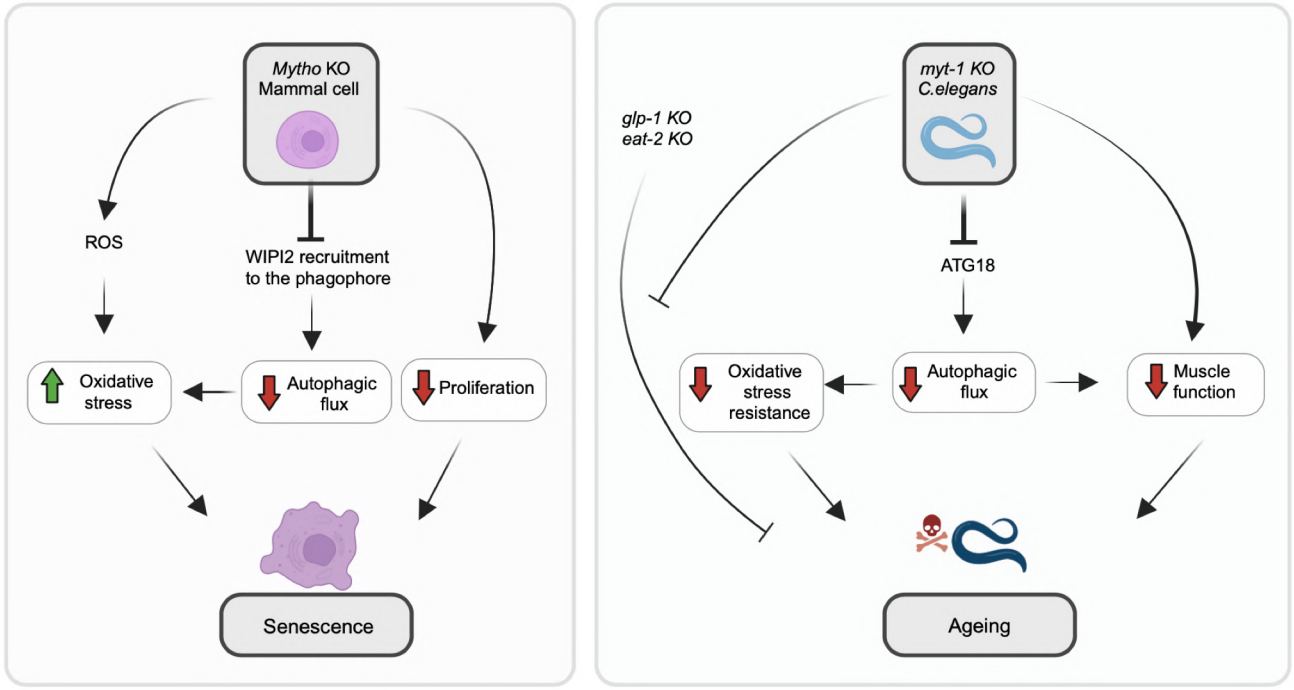
Mytho KO
Mammal cell
ROS
WIPI2 recruitment
to the phagophore
Oxidative
stress
Autophagic
flux
Proliferation
Senescence
myt-1 KO
C.elegans
glp-1 KO
eat-2 KO
ATG18
Oxidative
stress
resistance
Autophagic
flux
Muscle
function
Ageing